CAIT-UTC-015

Combining Model Based and Data Based Techniques in a Robust Bridge Health Monitoring Algorithm

Final Report
September 2014

Raimondo Betti
Professor
Columbia University
New York NY 10027

External Project Manager
Dyab Khazam
Parsons Transportation Group

In cooperation with
Rutgers, The State University of New Jersey
And
State of New York
Department of Transportation
And
U.S. Department of Transportation
Federal Highway Administration

Disclaimer Statement

TECHNICAL REPORT STANDARD TITLE PAGE

1. Report No.	2. Government Accession No.	3. Recipient's Catalog No.
CAIT-UTC-015		

4. Title and Subtitle	5. Report Date
Combining Model Based and Data Based Techniques in a Robust Bridge Health Monitoring Program	September 2014
	6. Performing Organization Code CAIT/Columbia University

7. Author(s)	8. Performing Organization Report No.
Raimondo Betti	CAIT-UTC-015

9. Performing Organization, Name and Address	10. Work Unit No.
Department of Civil & Environmental Engineering Columbia University New York NY 10027	
	11. Contract or Grant No. DTRT12-G-UTC16

12. Sponsoring Agency Name and Address	13. Type of Report and Period Covered
Center for Advanced Infrastructure and Transportation Rutgers, The State University of New Jersey 100 Brett Road Piscataway, NJ 08854	Final Report 11/1/12 - 8/30/2014
	14. Sponsoring Agency Code

15. Supplementary Notes

U.S Department of Transportation/Research and Innovative Technology Administration
1200 New Jersey Avenue, SE
Washington, DC 20590-0001

16. Abstract

Structural Health Monitoring (SHM) aims to analyze civil, mechanical and aerospace systems in order to assess incipient damage occurrence. In this project, we are concerned with the development of an algorithm within the SHM paradigm for application to civil engineering structures. Vibration-based techniques are the ones considered to be the most appropriate to perform SHM of civil engineering structures. They are based on the premise that damage will alter the properties of the structure, which will be manifested in its dynamic response. Thus, by measuring and analyzing the vibration response time histories it will be possible to detect such changes.

A "mixed" approach to vibration based SHM is explored in this project, combining the comparative advantages provided by "model based" and solely "data based" techniques. A damage sensitive feature (DSF) is defined using experimental modal parameters which may be obtained from operational/ambient vibration response of the structure. This DSF is proportional to the relative change in any diagonal element of the stiffness matrix of a model of the structure, with structural damage being represented as localized stiffness reduction. Although the DSF is derived in a model-based setting, necessary parametric modeling assumptions are kept to a minimum. The DSFs extracted from measured vibration response data are used to perform damage assessment in a statistical pattern recognition (data-based) framework, using empirical complementary cumulative distribution functions (ECCDFs) of the DSFs. The inherent statistical nature of the framework allows for uncertainties induced by measurement noise, environmental/ambient effects etc. Methods are discussed to perform a three-fold probabilistic structural health assessment: (a) "Is there a change in the current state of the structure compared to the baseline state?", (b) "Does the change indicate a localized stiffness reduction or increase?", with the latter representing a situation of verification of retrofitting operations, and (c) "What is the severity of the change in a probabilistic sense?". Particular effort is made to account for "non-damage" related structural variations, induced, for example, by diurnal temperature changes, using lower and upper bound ECCDFs to define the baseline structural state. Such an approach is intended to decouple normal structural variations from damage induced changes. The damage assessment procedure is discussed using numerical simulations of ambient vibration testing of a bridge deck system, considering both complete and partial instrumentation scenarios.

17. Key Words	18 Distributional Statement
Structural Health Monitoring, Vibration	

19. Security Classification	20. Security Classification (of this page)	21. No. of Pages	22. Price
Unclassified	Unclassified	59	

Form DOT F 1700.7 (8-09)

Contents

Executive Summary

Structural Health Monitoring (SHM) aims to analyze civil, mechanical and aerospace systems in order to assess incipient damage occurrence. In this project, we are concerned with the development of an algorithm within the SHM paradigm for application to civil engineering structures. Vibration-based techniques are the ones considered to be the most appropriate to perform SHM of civil engineering structures. They are based on the premise that damage will alter the properties of the structure, which will be manifested in its dynamic response. Thus, by measuring and analyzing the vibration response time histories it will be possible to detect such changes.

A "mixed" approach to vibration based SHM is explored in this project, combining the comparative advantages provided by "model based" and *solely* "data based" techniques. A damage sensitive feature (DSF) is defined using experimental modal parameters which may be obtained from operational/ambient vibration response of the structure. This DSF is proportional to the relative change in any diagonal element of the stiffness matrix of a model of the structure, with structural damage being represented as localized stiffness reduction. Although the DSF is derived in a model-based setting, necessary parametric modeling assumptions are kept to a minimum. The DSFs extracted from measured vibration response data are used to perform damage assessment in a statistical pattern recognition (data-based) framework, using empirical complementary cumulative distribution functions (ECCDFs) of the DSFs. The inherent statistical nature of the framework allows for uncertainties induced by measurement noise, environmental/ambient effects etc. Methods are discussed to perform a three-fold probabilistic structural health assessment: (a) "Is there a change in the current state of the structure compared to the baseline state?", (b) "Does the change indicate a localized stiffness reduction or increase?", with the latter representing a situation of verification of retrofitting operations, and (c) "What is the severity of the change in a probabilistic sense?". Particular effort is made to account for "non-damage" related structural variations, induced, for example, by diurnal temperature changes, using lower and upper bound ECCDFs to

define the baseline structural state. Such an approach is intended to decouple normal structural variations from damage induced changes. The damage assessment procedure is discussed using numerical simulations of ambient vibration testing of a bridge deck system, considering both complete and partial instrumentation scenarios.

1. Introduction

Structural Health Monitoring (SHM) is the task of evaluating the current condition of a structural system, e.g. a building or a bridge in civil engineering applications, to establish whether the system can be considered "healthy" to meet its daily operational requirements. In case the evaluation results in declaring the system to be "damaged", then SHM may also be used in planning and validating the necessary retrofitting operations. With the national infrastructure rapidly decaying because of lack of resources and/or proper maintenance, a successful SHM strategy is of paramount interest to engineers and government authorities responsible for the continuous functionality of complex structural systems such as bridges. In today's world, bridges play a vital role in the urban landscape (e.g. nearly 90 percent of the national food chain moves on state bridges) and hence need to be kept constantly operational so as to prevent disruption to large sectors of our society. However, according to the latest report of the American Society of Civil Engineers, about 25 percent of the entire national bridge inventory comprises bridges that are either structurally deficient or functionally obsolete. In about 15 years, 50 percent of this nation's bridges will be over 50 years old and this will imply an unprecedented commitment of both financial and human resources. Consequently, there will be the need for more reliable, economic and easy to conduct inspections that can take advantage of the many advances in other areas, like computer technology, material science and statistics. It is in this framework that the concept of SHM needs to be framed. Thanks to the latest innovations in computer and sensor technology, it is now possible to collect large amounts of data that represent the response of the bridge to the environment excitation and, through the analysis of such data, to provide an instantaneous assessment of the bridge conditions.

Current research efforts in vibration based SHM usually involve either "model based" or "data

based" techniques. Both these classes of methods have their own domains of comparative advantages and disadvantages. Model based methods involve solving an inverse problem, where the parameters of an assumed analytical model of the true physical system are identified/updated, either directly or iteratively, such that the response of the identified/updated model mimics the measured response from the real structure. While the identification of an *accurate* parametric model of the structure will allow the identification of the existence, location and severity of structural damage, *accurate* models of true physical systems seldom exist in practice. Moreover, both deterministic as well as stochastic (accounting for modeling assumption, environmental variation, measurement noise etc. induced uncertainties) model updating/identification techniques usually involve the solution of some nonlinear optimization problem(s), and they can efficiently handle the problem only when a limited number of model parameters are to be optimized (identified). This necessitates a considerable amount of reliability in the *a priori* analytical model. In situations where the representative model may not be very reliable, and this is often the case for large and complicated systems, the model-based health monitoring procedure should treat all the model parameters as unknown. However, applying conventional model based techniques to large and complicated systems will, firstly, prove inefficient if one treats all/most of the model parameters as unknowns/uncertain, and secondly, may not converge at all to a unique identified/updated system [1–4].

As an alternative, solely data-based methods do not require any *a priori* definition of *accurate* physical models of the structure, and instead rely exclusively on the data recorded from the true structure [5, 6]. Hence, such methods circumvent the inevitable uncertainties induced by assumptions in any parametric model-based technique. In essence, these methods attempt to identify patterns characterizing the structure by analyzing the recorded vibration signatures of the structure, thus also classifying them as "pattern recognition" based methods, implemented in a statistical pattern recognition framework. In structural damage detection, these patterns are called *damage sensitive features* (DSF), which are quantities that indicate the presence of damage in a structure [6]. Hence, an appropriate DSF should be sensitive to structural damage, which in turn is related to changes in the structural properties. However, the structural properties also vary due to fluctu-

ations in environmental and operational conditions. Therefore, a good DSF should be sensitive to changes in the structural properties induced by damage while being insensitive to variations due to non-damage related conditions. In order to learn the typical variations in the DSFs induced by external factors, the DSFs extracted from the measured responses of the baseline (healthy) structure under different environmental/operational conditions are first used to construct a baseline statistical model of the DSFs (training). Such a model represents statistically the *normal* fluctuations that the DSFs will experience; any variation beyond this normal range will signal damage occurrence. Once the training model is built, the DSFs extracted from any new measured response of the structure (healthy or damaged) can be compared to the baseline statistical model (testing) to identify whether the structure is still in a healthy state or has undergone any deterioration/damage. The inherent statistical nature of the pattern recognition framework also allows one to account for uncertainties induced by measurement noise, input variability, etc. In spite of the above apparent advantages of such methods, contributing to their general robustness in structural damage identification, the performance of any particular method within this framework in successfully locating and quantifying damage depends on the particular damage sensitive feature used. Due to the choice of the damage sensitive features, which are often selected as abstract information not explicitly related to the physical properties of the system, traditional damage detection algorithms developed within the statistical pattern recognition framework can seldom locate and quantify damage, although they can accurately distinguish between a "damaged" and a "healthy" structural system. Moreover, in SHM applications to buildings and bridges, measured data from different damage states of the true system are not available in practice, and hence the statistical pattern recognition approach is implemented in what is called an *unsupervised* learning mode. (The term *unsupervised* is used to denote the lack of data recorded from any damage state of the structure during training, as opposed to *supervised* learning where data from both healthy and damage conditions are used to build the training model.) Thus, the solution to the damage detection problem ends up assigning the new measured data to one of two classes: the *previously learnt* (healthy) class, or a *never seen before* (damaged) class; questions on the type, location and severity of the damage are usually left

unanswered.

Some other challenges in data-based methods include the selection of an appropriate statistical model for the DSFs, and of an appropriate metric to measure the "distance" of newly extracted features from the baseline statistical model. While normally distributed features and the squared Mahalanobis distance (SMD) metric are popular choices [7, 8], the normal distribution assumption may be erroneous, especially when the number of available observations (size of the measured training data set) is not large. (In case of large civil structures, the costs of instrumentation and data storage/data processing, faulty instruments etc. may create situations of limited training data.) Moreover, in such cases of small sample training data set, the estimation of a well-conditioned covariance matrix for evaluating the SMD metric, as well as threshold selection for damage detection using the SMD metric, may require special treatments [9].

In view of the aforementioned reasons, we pursue a "mixed" approach in this study, attempting to combine the comparative advantages of model-based and data-based techniques into a robust vibration based continuous SHM strategy. Due to their intuitive relationship with the structural topology and characteristics, modal properties, especially when in the form of mode shapes, can be expected to solve the problems of damage location and severity quantification, if a modal parameter based damage sensitive feature is so defined as to be tailored to that purpose. In fact, several studies in the past have addressed the problem of structural damage detection using modal parameters, either through some direct comparative measures, or in conjunction with some model-related assumptions (e.g. the mass matrices of the damaged and undamaged systems' models are the same etc.) to estimate damage induced changes in element stiffnesses/flexibilities [10–14]. While modal frequencies, a global dynamic property of the structure, are usually relatively insensitive to local structural damage, mode shapes, being "spatially distributed" features, contain information which may be employed for damage location purposes. Although the direct comparison of mode shapes using inner product norms to test their linear dependence (Cauchy-Schwarz inequality), as in the Modal Assurance Criterion/Coordinate Modal Assurance Criterion, seems an obvious approach and has often been adopted in the literature, the differences reflected by such measures can

be expected to be of a lower order than the actual differences in the structural flexibility matrix [15]; thus, for the purpose of structural damage detection, the use of such measures may not provide sufficiently discernible results. Instead, in [15, 16] modal parameter comparative measures are derived which mimic changes in the structural flexibility and stiffness matrices. This report is based on the DSF introduced in [16], which gives a measure of the relative difference between the corresponding diagonal elements of the stiffness matrices of the models of two systems at comparison. The DSF is defined in terms of the experimental modal parameters, which may be identified from the ambient/operational response of the monitored structural system using any operational modal analysis technique. To obtain normalized mode shapes, it is usually necessary to know the applied input(s) and have at least one pair of sensor and actuator placed at the same location on the monitored system [3]; since we consider here the more feasible operational testing scenario (output-only data), the identified experimental mode shapes will need to be normalized following an alternative approach. For this purpose, a procedure is discussed to estimate proportional mass normalizing factors, using the sparsity requirement of the mass matrix at the measurement locations. Although the derivation of the DSF and the mode shape normalization are performed in a model-based setting, as will be evident later, we keep the necessary parametric modeling assumptions to a minimum, and in fact do not require the *a priori* knowledge of any mass/stiffness parameter values. The mode shape normalization and DSF computation are discussed in Section 2.

While the definition of the DSF is in a model-based framework, the damage assessment procedure, using the DSFs extracted from measured vibration response data, is developed according to the statistical pattern recognition paradigm. The empirical complementary cumulative distribution functions (ECCDFs) of the extracted DSFs are computed for that purpose; damage assessment is performed by comparing the ECCDFs obtained during the testing stage with the ECDDFs created during the training stage. The statistical modeling of the DSFs using ECCDFs avoid the assumption of any particular type of parametric distribution to statistically model the DSFs, and hence may be expected to provide a more robust damage assessment. The proposed structural health as-

sessment approach attempts to answer three questions: (1) "Is there a change in the current state of the structure compared to the baseline state?", (2) "Does the change indicate a localized stiffness reduction or increase (in case of retrofitting)?", and (3) "What is the severity of the change in a probabilistic sense?". The possible scenario of localized stiffness increase is also included, and is intended for applications in which the success of planned retrofitting operations need to be verified [17, 18]; three ratios of the Łukaszyk–Karmowski metric ([19]) are used, with the empirical probability density functions (epdfs) derived from the ECCDFs of the DSFs, to distinguish between localized stiffness increase (retrofit) and decrease (damage). For the purpose of damage severity estimation, damage probability vs. damage severity curves are derived from the ECCDFs [20].

It has been widely reported in the literature that modal parameters are significantly affected by "non-damage" related structural variations, induced, for example, by temperature changes, or other environmental/operational fluctuations [21–24]. Hence, in the entire damage assessment approach discussed here, such effects are particularly taken into account using lower and upper bound ECCDFs to define the baseline structural state; these lower and upper bounds are obtained using training response time histories measured in different environmental conditions. Such an approach is intended to decouple normal structural variations from damage induced changes. The lower and upper bound baseline ECCDFs are also used to quantify the uncertainty in the damage probability - damage severity curves; the two-level uncertainty in the damage severity may be expected to include both statistical (epistemic) uncertainty induced by measurement noise, estimation errors, input variability etc., as well as systematic (aleatoric) uncertainty induced by unmeasured variables (e.g. temperature). The derivation of the training and testing ECCDFs of the DSFs are discussed in Section 3, and the different levels of damage assessment using the ECCDFs are discussed in Section 4 using numerical simulations of ambient vibration testing of a bridge deck system, considering both complete and partial instrumentation scenarios.

2. SPDSF: Stiffness Proportional Damage Sensitive Feature

In SHM structural damage is often modeled as localized stiffness reduction. Therefore, constructing a DSF which measures the deviation of the stiffness properties from a reference baseline state may be expected to deliver optimal results in damage detection. In order to define such a feature, let us consider an N degrees of freedom (DOF) classically damped model of a system, whose dynamic behavior is governed by the equation of motion:

$$\mathbf{M}\ddot{\mathbf{y}} + \mathbf{L}\dot{\mathbf{y}} + \mathbf{K}\mathbf{y} = \mathbf{u} \tag{2.1}$$

where $\mathbf{M}$, $\mathbf{L}$ and $\mathbf{K}$ are respectively the $N \times N$ mass, damping and stiffness matrices of the model, $\mathbf{y}$, $\dot{\mathbf{y}}$ and $\ddot{\mathbf{y}}$ denote respectively the nodal displacement, velocity and acceleration vectors of dimension $N \times 1$, and $\mathbf{u}$ is the $N \times 1$ dimensional input dynamic forcing vector. Let the state of the system described by Eq. (2.1) and the above model matrices be the baseline (healthy) state. Next, let us consider an alternative state of the system denoted by the matrices: $\{\mathbf{M}^*, \mathbf{L}^*, \mathbf{K}^*\}$. This alternative state represents the system in an unknown condition, either damaged or same as the baseline, and its dynamic behavior will still be governed by a similar equation as Eq. (2.1). Using these notations, the damage sensitive feature discussed here attempts to measure the departure of the $\{i, i\}^{th}$ element of $\mathbf{K}^*$ from the $\{i, i\}^{th}$ element of $\mathbf{K}$:

$$\text{DSF}_i = \frac{K_{i,i} - K^*_{i,i}}{K_{i,i}} \tag{2.2}$$

where the subscripts indicate the row and column numbers, respectively. Now, let us denote by $\{\mathbf{\Lambda}, \mathbf{\Phi}\}$ the eigenvalue and eigenvector matrices corresponding to the baseline state:

$$\mathbf{\Lambda} = \text{diag}\big(\lambda_1, \lambda_2, \cdots, \lambda_N\big) = 4\pi^2 \text{diag}\big(f_1^2, f_2^2, \cdots, f_N^2\big) \tag{2.3}$$

$$\mathbf{\Phi} = [\boldsymbol{\phi}_1 \quad \boldsymbol{\phi}_2 \quad \cdots \quad \boldsymbol{\phi}_N] = \begin{bmatrix} \phi_{1,1} & \phi_{1,2} & \cdots & \phi_{1,N} \\ \phi_{2,1} & \phi_{2,2} & \cdots & \phi_{2,N} \\ \vdots & \vdots & \ddots & \vdots \\ \phi_{N,1} & \phi_{N,2} & \cdots & \phi_{N,N} \end{bmatrix} \tag{2.4}$$

where λ_j, f_j and the column vector $\boldsymbol{\phi}_j$ denote the jth modal eigenvalue, frequency and mode shape, respectively, while $\phi_{i,j}$ denotes the ith component (corresponding to DOF i) of $\boldsymbol{\phi}_j$. The scenario considered in this project is that of ambient/operational monitoring, and hence the input $\mathbf{u}$ in Eq. (2.1) is unknown, and only the output responses are measured at all DOFs (full instrumentation) or at only a subset of the N DOFs (partial instrumentation). In such a situation, the identified experimental mode shapes are, in general, arbitrary scaled. Such a set of arbitrarily scaled complete mode shapes will then satisfy the orthogonality relations:

$$\mathbf{\Phi}^T \mathbf{M} \mathbf{\Phi} = \boldsymbol{\alpha}; \quad \mathbf{\Phi}^T \mathbf{K} \mathbf{\Phi} = \mathbf{\Lambda} \boldsymbol{\alpha} \tag{2.5}$$

where $\boldsymbol{\alpha}$ is a diagonal matrix containing the squares of the normalization factors: $\boldsymbol{\alpha} = \text{diag}(\alpha_1, \alpha_2, \cdots, \alpha_N)$. As for the physical matrices, let $\{\mathbf{\Lambda}^*, \mathbf{\Phi}^*, \boldsymbol{\alpha}^*\}$ denote the eigenvalue, eigenvector, and normalizing factor matrices of the alternative state of the system. Then, defining the matrices: $\mathbf{A} = \mathbf{M}^{-1}\mathbf{K}\mathbf{M}^{-1}$, and $\mathbf{A}^* = \mathbf{M}^{*-1}\mathbf{K}^*\mathbf{M}^{*-1}$, a DSF similar to the one in Eq. (2.2) may be defined and written in terms of the modal parameters as:

$$\widetilde{\text{DSF}}_i = \frac{A_{i,i} - A^*_{i,i}}{A_{i,i}} = 1 - \frac{\sum_{j=1}^{N} \phi^{*2}_{i,j} \lambda^*_j \alpha^{*-1}_j}{\sum_{j=1}^{N} \phi^2_{i,j} \lambda_j \alpha_j^{-1}} \tag{2.6}$$

While the DSF of Eq. (2.6) has the obvious advantage of being applicable for general systems, it will be able to detect damage (stiffness reduction) accurately under the condition that $\mathbf{M} \approx \mathbf{M}^*$; although damage may not affect the system's mass in any noticeable extent, the mass matrices in the two states, $\mathbf{M}$ and $\mathbf{M}^*$, can still be different due to environmental (e.g. humidity) or operational (traffic on a bridge) variability. As an alternative, one can go from the DSF in Eq. (2.6) to the DSF in Eq. (2.2), at the cost of the assumption of a lumped mass matrix (i.e. $\mathbf{M}$ and $\mathbf{M}^*$ are diagonal), with the DSF in Eq. (2.2) then written in terms of the experimental modal parameters as:

$$\text{DSF}_i = 1 - \frac{\left(\sum_{j=1}^{N} \phi_{i,j}^2 \alpha_j^{-1}\right)^2 \left(\sum_{j=1}^{N} \phi_{i,j}^{*2} \lambda_j^* \alpha_j^{*-1}\right)}{\left(\sum_{j=1}^{N} \phi_{i,j}^{*2} \alpha_j^{*-1}\right)^2 \left(\sum_{j=1}^{N} \phi_{i,j}^2 \lambda_j \alpha_j^{-1}\right)} \tag{2.7}$$

In this project, we consider systems which can be represented through lumped mass models, and hence we will use the DSFs in Eq. (2.7). Since this DSF measures the relative change in the system's local stiffness properties compared to the benchmark state, it is referred to as *Stiffness Proportional Damage Sensitive Feature* (SPDSF). Note that, even though the DSFs in both Eqs. (2.6) and (2.7) are written for an identified complete spectrum, since the summations in these equations are performed over the modes (i.e. index i = mode number), in situations where only N_m modes are identified from the data, the DSFs may still be computed using only these N_m modes in the summations.

While any appropriate operational modal analysis technique may be used with the measured response data to identify the system's frequencies (or eigenvalues) and the mode shapes at the sensor locations, the normalizing factors in $\boldsymbol{\alpha}$ and $\boldsymbol{\alpha}^*$ necessary in Eq. (2.7) (or Eq. (2.6)) still need to be evaluated. One may employ the topological requirements of the $\mathbf{M}$ and $\mathbf{K}$ matrices for this purpose [4]. Since we consider here systems with general (may be completely populated) $\mathbf{K}$ matrices, we will not use any requirement (e.g. sparsity or connectivity) posed by the $\mathbf{K}$ matrix. Instead, we will use the sparsity requirement of diagonal (lumped) $\mathbf{M}$ matrices to estimate the normalizing factors. As proved in [4], in output only situations, for models with diagonal $\mathbf{M}$, with sufficient instrumentation to enable a unique mode shape expansion, one can only identify a model

proportional to the true model by a single scalar factor, without using any *a priori* knowledge of the value of any physical parameter. This means we will be able to identify uniquely only $(N-1)$ normalizing factors using the sparsity of $\mathbf{M}$. Let us then rewrite the matrix of normalizing factors by factoring out the first element α_1 as: $\boldsymbol{\alpha} = \alpha_1 \text{diag}(\beta_1 = 1, \beta_2, \cdots, \beta_N)$, where $\beta_j = \alpha_j/\alpha_1$. The *proportional* normalizing factors $\{\beta_2, \cdots, \beta_N\}$ can then be estimated by solving the following linear system of equations (depicting the sparsity of $\mathbf{M}$) in the least squares sense:

$$\sum_{j=1}^{N} \frac{\phi_{i,j}\phi_{l,j}}{\beta_j} = -\phi_{i,1}\phi_{l,1}, \qquad \text{for } i, l \in \mathcal{S} \text{ and } i \neq l \tag{2.8}$$

where $\mathcal{S}$ is the set of instrumented DOFs. If the system is instrumented with N_s sensors (i.e. N_s elements in $\mathcal{S}$), Eq. (2.8) will constitute a set of $(N_s^2 - N_s)/2$ equations, thereby leading to the minimal instrumentation requirement of $N_s \geq (1 + \sqrt{8N-7})/2$ to be able to uniquely estimate all the $(N-1)$ β_j's. (However, any random location of the N_s sensors may not provide a unique estimate; the reader is referred to [4] for more details on instrumentation requirements for global identifiability.) Similarly, the $(N-1)$ β_j^*'s can be solved using the identified modal parameters of the alternative state of the system. Then, the DSF of Eq. (2.7) can be rewritten as:

$$\text{DSF}_i = 1 - \frac{\alpha_1^*}{\alpha_1} \frac{\left(\sum_{j=1}^{N} \phi_{i,j}^2 \beta_j^{-1}\right)^2 \left(\sum_{j=1}^{N} \phi_{i,j}^{*2} \lambda_j^* \beta_j^{*-1}\right)}{\left(\sum_{j=1}^{N} \phi_{i,j}^{*2} \beta_j^{*-1}\right)^2 \left(\sum_{j=1}^{N} \phi_{i,j}^2 \lambda_j \beta_j^{-1}\right)} \tag{2.9}$$

where, to evaluate the ratio α_1^*/α_1, one would need some assumption on the value of any physical parameter of the system. If the assumption is made that the change in the total mass (= sum of all element masses) of the system in its transition from one state to another is minimum, then this ratio may be estimated as:

$$\frac{\alpha_1^*}{\alpha_1} = \underset{\alpha_1^*/\alpha_1}{\arg\min} \left(\sum_{i=1}^{N} \left(M_{i,i} - M_{i,i}^* \right) \right)^2 = \frac{\sum_{i=1}^{N} \left(\sum_{j=1}^{N} \phi_{i,j}^2 \beta_j^{-1} \right)}{\sum_{i=1}^{N} \left(\sum_{j=1}^{N} \phi_{i,j}^{*2} \beta_j^{*-1} \right)} \tag{2.10}$$

In the rest of the report the DSFs used will be evaluated using Eq. (2.9), along with Eqs. (2.8)

and (2.10). Even though the DSF in Eq. (2.9) is written for an identified complete spectrum, in situations where only $N_m < N$ modes are identified from the data, the DSF may still be computed using only these N_m modes in the summation. However, in order to identify the normalizing factors though Eqs. (2.8) and (2.10), all N modes need to be identified at the sensor locations; if $N_m < N$ modes are identified then other approaches may be used to compute these factors [25]. Since the DSFs discussed herein are particular to the different DOFs constituting the model of the system, these DSFs may be used not only to test for the existence of damage in the system, but also to locate the damage to the neighbourhood of any particular DOF. Moreover, since the DSFs provide a measure of the relative change, with respect to the baseline state, in the diagonal elements of the stiffness matrix, they may also be used to assess the severity of any localized damage.

3. Empirical Complementary Cumulative Distributions of SPDSF

Inherent in the definition of the DSFs in Section 2 is a comparison between two states of the system, unlike traditional DSFs which represent a single state of the system. For example, a change in the stiffness of an element connecting nodes i and l would be reflected in a change in the values of the ith and lth elements in the main diagonal of $\mathbf{K}$, and this change would be captured by DSF_i and DSF_l. However, as discussed in Section 1, changes in structural properties may also be introduced by factors other than damage. The DSFs of Section 2 will not only measure the change in the stiffness properties induced by structural damage, but will also measure stiffness changes induced by environmental and operational variability. It is pertinent that the damage detection procedure be able to distinguish between the damage induced and non-damage induced fluctuations in the DSFs, so as to reduce instances of *false alarms* and *false safety*. This requirement defines an objective of the training phase: to define boundaries for the fluctuations of the DSFs that can be considered normal (non-damage induced), and thereby define a reference "healthy" zone against which new realizations of the DSFs, extracted from the system under unknown conditions, can be compared. To this end, we use the cumulative distribution functions (CDFs) of the DSFs, treating each DSF as a random variable, as discussed below.

It is possible to cast the SHM problem in a probabilistic framework by introducing the "probability of damage" assigned to any model parameter [14, 20]. In the context of this report, such a probability can be assigned to each diagonal element of $\mathbf{K}$, and be defined as the probability that the $\{i, i\}$th element, $K^*_{i,i}$, of the stiffness matrix in an unknown (possibly damaged) state be less

than a prescribed fraction of the same element, $K_{i,i}$, in the baseline (healthy) state:

$$P_i^{\text{damage}}(d) = P(K_{i,i}^* \leq (1-d)K_{i,i}) \quad \text{for } d \in [0,1) \tag{3.1}$$

where d is the fractional stiffness reduction (damage). Eq. (3.1) can be rewritten using the DSF defined in Section 2 as:

$$\begin{aligned} P_{DSF_i}^{\text{damage}}(d) &= P\left(\frac{K_{i,i} - K_{i,i}^*}{K_{i,i}} \geq d\right) && (3.2)\\ &= 1 - P\left(\frac{K_{i,i} - K_{i,i}^*}{K_{i,i}} \leq d\right) && (3.3)\\ &= 1 - \text{CDF}_{DSF_i}(d) && (3.4) \end{aligned}$$

The training procedure to build statistical models of the baseline state's DSFs, encompassing the normal variability of the CDFs of the DSFs, can then be performed as discussed herein. Let n_{tr} denote the number of measurement campaigns (= number of sets of measured response data) that have been conducted on the monitored system under *different healthy conditions*; these *different healthy conditions* includes different environmental and operational conditions of the healthy state of the system. For example, data collected during different periods of the year may represent the different environmental conditions, while data recorded under different traffic conditions will depict different operational conditions. Also let N_s be the number of sensors used in each measurement campaign, and $\mathcal{S}$ be the set of the N_s measured DOFs. From such measurements, a set $Y = \{\mathbf{\Lambda}^{(p)}, \mathbf{\Phi}^{(p)}\}$, for $p = 1, \cdots, n_{tr}$, of modal parameters may be identified, where $\mathbf{\Lambda}^{(p)} \in \mathbb{R}^{N \times N}$ and $\mathbf{\Phi}^{(p)} \in \mathbb{R}^{N_s \times N}$ are the pth realizations (i.e. identified from the pth set of measured response data) of the eigenvalue (squared circular modal frequency) and mode shape matrices, respectively. The set Y is then divided into two subsets Y_H and Y_V such that:

$$Y_H \cup Y_V = Y; \quad Y_H \cap Y_V = \emptyset; \quad Y_H, Y_V \neq \emptyset; \quad |Y_H| = n_H; \quad |Y_V| = n_V \tag{3.5}$$

Now, the identified modal parameters contained in the set Y_H are considered as reference, while

those in the set Y_V are considered to come from an unknown state of the system, i.e., following the terminology used in Section 2, Y_H corresponds to the baseline state while Y_V corresponds to the the alternative state (although both these sets contain modal information of the healthy state of the system). Then, each set of modal parameters in Y_V is compared with each and every set of modal parameters in Y_H using the DSF of Eq. (2.9); this results in a total of n_V sets, each set containing n_H values, of DSF_i, for all $i \in \mathcal{S}$. Empirical cumulative distribution functions (ECDFs) of DSF_i are then computed using Eq. (3.6) [26], for each of these n_V sets, treating the n_H DSF_i values in each set ($\text{DSF}_i^{p,j}$ for $p = 1, \cdots, n_H$) as random realizations:

$$\text{ECDF}^j_{\text{DSF}_i}(d) = \frac{1}{n_H} \sum_{p=1}^{n_H} U(d - \text{DSF}_i^{p,j}) \quad \forall\, j = 1, \cdots, n_V \text{ and } i = 1, \cdots, N_s \tag{3.6}$$

where $U(z)$ is the Heaviside function:

$$U(z) = \begin{cases} 0 & z < 0 \\ 0.5 & z = 0 \\ 1 & z > 0. \end{cases} \tag{3.7}$$

and $\text{DSF}_i^{p,j}$ denotes the DSF corresponding to the DOF measured by sensor i and obtained comparing the jth modal parameter set from Y_V to the pth modal parameter set from Y_H.

The $\text{ECDF}^j_{\text{DSF}_i}(d)$ in Eq. (3.6) can be substituted in place of $\text{CDF}_{\text{DSF}_i}(d)$ in Eq. (3.2); the resulting $P_i^{\text{damage}}(d)$ in Eq. (3.2), computed as $1 - \text{ECDF}^j_{\text{DSF}_i}(d)$, is then referred to as the *Empirical Complementary Cumulative Distribution Function* (ECCDF) of DSF_i (i.e. $\text{ECCDF}^j_{\text{DSF}_i}(d)$). In this way, we get n_V number of curves representing $\text{ECCDF}_{\text{DSF}_i}(d)$, for each $i \in \mathcal{S}$. The maximum and minimum bounds of these n_V number of $\text{ECCDF}_{\text{DSF}_i}(d) = P_i^{\text{damage}}(d)$ are then computed, to estimate an acceptable range of d, denoting normal environmental/operational variability. These lower and upper bound ECCDFs also define the lower and upper bound probabilities associated with each value of d in this range, for each DSF_i, $i \in \mathcal{S}$.

At the time of testing, a new set of response data is measured with the N_s sensors from the structure under unknown conditions, and a single set of modal parameters is identified from this data set. This new set of modal parameters is compared to each and every of the n_H sets of modal parameters in Y_H obtained during the training stage, with the new set and the n_H training sets respectively corresponding to the alternative state and the baseline state as per the terminology in Section 2. The resulting n_H values of DSF_i are then used to compute a single $\text{ECCDF}_{\text{DSF}_i}(d)$, following the procedure outlined in the training stage, for every $i \in \mathcal{S}$. This single $\text{ECCDF}_{\text{DSF}_i}(d)$ is then compared with the lower and upper bounds of $\text{ECCDF}_{\text{DSF}_i}(d)$ obtained during the training stage for damage assessment purposes. This comparison may be performed using different measures, with different objectives, which are discussed in the next section, using a numerical example for illustration purposes.

4. Different Levels Of Damage Assessment With Numerical Example

4.1 Numerical example description

To illustrate the different levels of the proposed damage assessment procedure, as well as to test its performance, we consider a simple lumped mass model of a bridge deck. This model constitutes of two interconnected spring-mass chains: each chain consists of alternately placed flexural links and lumped masses, with the corresponding lumped masses of the two chains being additionally connected by flexural links. Such a simple model can be used to represent simple overpasses or single spans of supported girder bridges, with the flexural links representing the various segments of the girders and the lumped masses the mass of the deck. Because of the structure of the model, its dynamic behavior will contain both global bending and global torsional modes of the deck. The particular model used in this project is shown in Fig. 4.1, and has 12 DOFs, with 12 lumped masses and 20 flexural links; the 12 vibration modes of this model (in the baseline state) are shown in Fig. 4.2, and represent 6 (dominantly) bending and 6 (dominantly) torsional modes. (The term "dominant" is used in the description of the modes, since the modes will be pure bending/torsion only for a symmetric mass/stiffness distribution; they will otherwise be coupled bending-torsion, with either bending/torsion dominating, as in all the numerical simulations performed in the project due to random parameter perturbations, environmental effects, damage etc.)

Table 4.1 lists the 10 different states considered here: the States 1 to 5 represent the healthy system, in different environmental conditions, the States 6 to 9 represent 4 different damaged states

with damages of different severities and in different elements, while State 10 represents the case where a certain portion of a girder is retrofitted leading to a stiffness increase in one of the flexural links. The baseline (State 1) model parameters are also given in Fig. 4.1, and the parameters in the other states are obtained from these baseline parameters.

In the training phase, 20 tests are performed on each of the 5 healthy states, 1 to 5: state 1 represents the baseline condition, states 2 and 3 represent environmental conditions where only the $-y$ side of the bridge is subjected to a temperature decrease/increase, while states 4 and 5 represent environmental conditions where only the $+y$ side of the bridge is subjected to a temperature decrease/increase. In each test the stiffness parameters defining the model are randomly perturbed: for any spring stiffness k_i, its value in the rth simulation is chosen as $k_i^r = E[k_i] + \mathcal{U}(-p_{k_i}, p_{k_i})E[k_i]$, where $E[k_i]$ is the mean value of that spring stiffness in that state (from Fig. 4.1 and Table 4.1), and $\mathcal{U}(l_l, l_r)$ is the uniform probability distribution between the limits l_l and l_r (p_{k_i} given in Fig. 4.1). While the change in the stiffness parameters given in Table 4.1 represents systematic changes, induced by temperature change, damage etc., and remain constant over all the 20 tests on the same state, the random perturbations with $\mathcal{U}(-p_{k_i}, p_{k_i})$ indicate statistical and inherent model/operational fluctuations within a state, and thus vary in the 20 different tests on the same state. The perturbed model in each test is excited by Gaussian white noise input forces applied at all the DOFs. The resulting "true" response accelerations are corrupted by adding 10% root mean square Gaussian white noise sequences (to simulate measurement noise) to get the "measured" acceleration responses at the instrumented DOFs. Two instrumentation set-ups are considered: (1) complete instrumentation, i.e. 12 sensors measuring the acceleration response of all the lumped masses, and (2) partial instrumentation, with 8 sensors, measuring the acceleration response of the 8 shaded lumped masses as shown in Fig. 4.1. The importance of considering partial instrumentation scenarios is that it is usually not feasible to instrument all the degrees of freedom in the system owing to limitations imposed by financial cost, data storage/processing costs, accessibility issues, etc. Such a partial instrumentation set-up has the advantage that all the springs' effects are being seen by the sensors; hence a damage in any of the 20 springs will be detected, and located to a

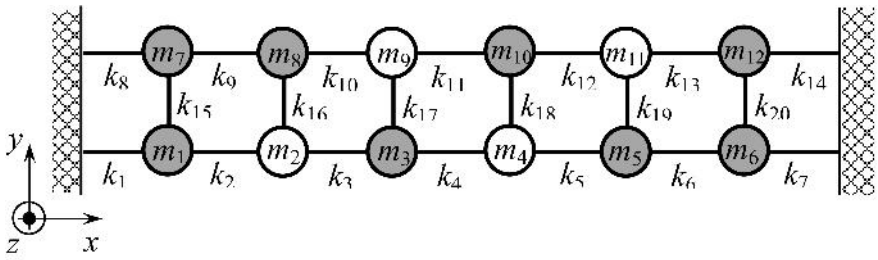

Baseline model parameters:
$m_i = 1.25\times10^5$ kg $\forall\ i \in \{1, \ldots, 12\}$
$E[k_i] = 7.12\times10^7$ N/m $\forall\ i \in \{1, \ldots, 20\}$
$p_{k_i} = 0.01\ \forall\ i \in \{1, \ldots, 20\}$
Rayleigh damping: $\zeta_1 = \zeta_2 = 0.01$

Figure 4.1: Bridge model and baseline model parameters used in numerical example. Shaded lumped masses denote sensor locations in partial instrumentation.

Table 4.1: Different states of the bridge deck structure considered in the example.

State	Condition	Description	Affected DOFs
1	Undamaged	Baseline condition	
2	Undamaged	$k_i = 0.99E[k_i]\ \forall i \in \{1, \cdots, 7\}$	
3	Undamaged	$k_i = 1.01E[k_i]\ \forall i \in \{1, \cdots, 7\}$	
4	Undamaged	$k_i = 0.99E[k_i]\ \forall i \in \{8, \cdots, 14\}$	
5	Undamaged	$k_i = 1.01E[k_i]\ \forall i \in \{8, \cdots, 14\}$	
6	Damaged	$k_1 = 0.70E[k_1]$	1
7	Damaged	$k_{16} = 0.80E[k_{16}]$	2 and 8
8	Damaged	$k_3 = 0.80E[k_3]$	2 and 3
9	Damaged	$k_3 = 0.70E[k_3]$	2 and 3
10	Retrofitted	$k_3 = 1.25E[k_3]$	2 and 3

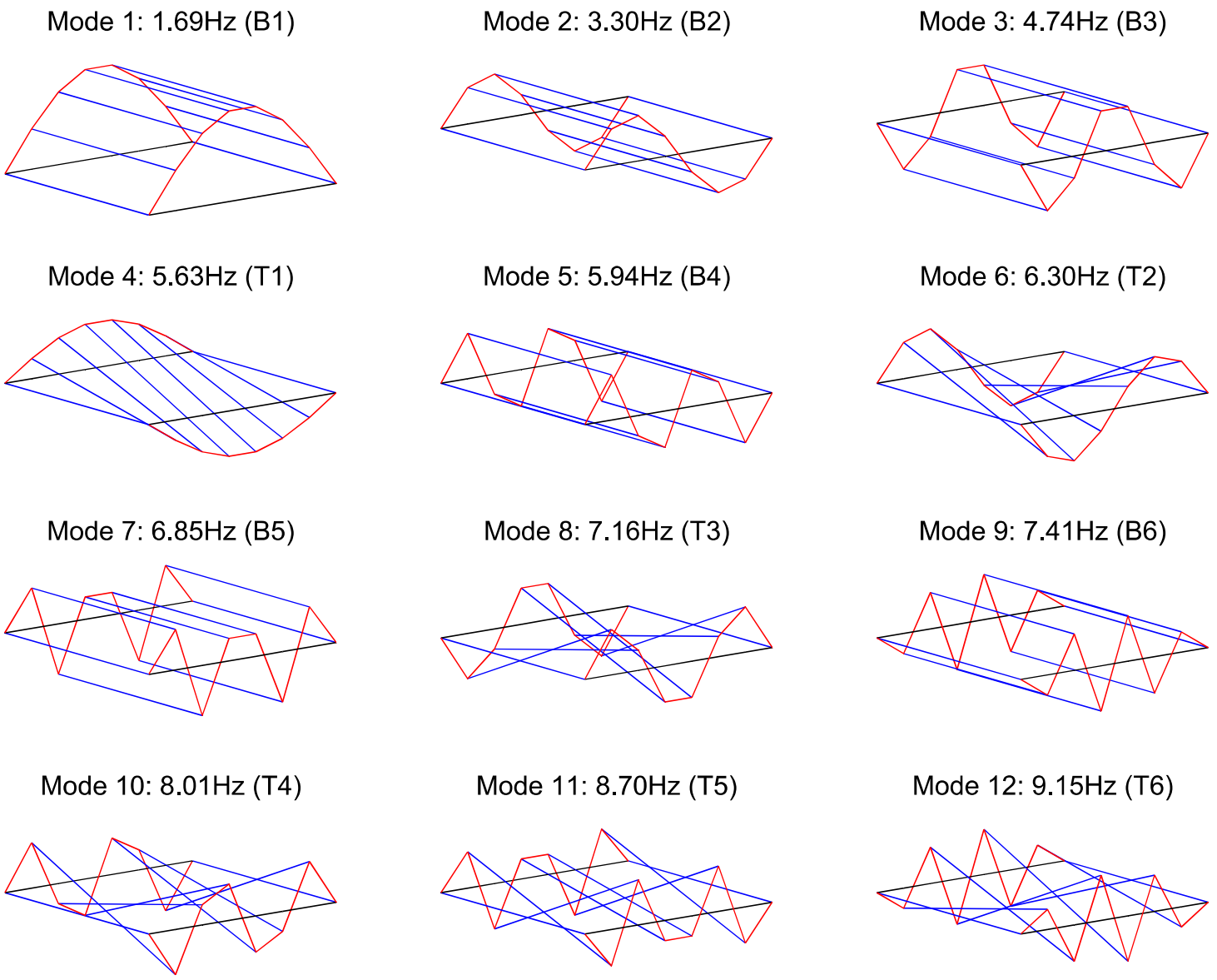

Figure 4.2: Analytical mode shapes of the mean baseline model (B: bending dominant mode; T: torsion dominant mode).

particular DOF. As discussed in Section 2, for a 12 DOF system, using only 6 sensors will be sufficient to estimate the 11 normalizing factors, and hence the DSFs at all the 6 instrumented DOFs. But in such a situation possible damages in some springs will go undetected; e.g. if we do not have sensors on m_6 and m_7, we will still be able to estimate $\{\text{DSF}_1, \text{DSF}_3, \text{DSF}_5, \text{DSF}_8, \text{DSF}_{10}, \text{DSF}_{12}\}$, but these will not capture the presence of possible damages in k_7 and k_8.

The set of "measured" acceleration responses in each test are used in a stochastic subspace identification algorithm, the Enhanced Canonical Correlation Analysis (ECCA) [27], which has shown great potential in separating noise modes from structural modes, to identify the modal frequencies and arbitrarily scaled mode shape components at the measured DOFs. With 20 tests per state, and 5 healthy states, the set Y in Section 3 consists of 100 sets ($n_{tr} = 100$) of identified training modal parameters; the subsets Y_H and Y_V are then constructed with 50 sets of modal parameters in each, 10 sets from each of the 5 states. Thus, both the subsets Y_H and Y_V contain information of all the systematic stiffness changes induced by environmental variability. The approach discussed in Sections 2 and 3 is then used to estimate the lower and upper bound ECCDFs of the DSFs at the measured DOFs. Figs. 4.3 and 4.4 show these lower and upper bound ECCDFs (thick red curves) of DSF_1 and DSF_3, obtained respectively in the full and partial instrumentation scenarios. (Note that these bounds are state-independent, since they are created using the training data, and use the extracted modal information from all the 5 healthy states together.)

In the testing phase, 10 tests are performed on each of the 10 states in Table 4.1, with each test simulated in the same way as in the training phase. The modal parameters identified through ECCA for each of these 10 tests (on any given state), are compared with the 50 sets of training modal parameters in Y_H, and the resulting 50 DSFs, at each of the measured DOFs, are used to construct the testing ECCDFs. Thus, with the 10 tests on each state, we get 10 testing ECCDFs of the DSFs at the measured DOFs for each state. Figs. 4.3 and 4.4 compare, respectively for the full and partial instrumentation scenarios, these 10 testing ECCDFs (thin black curves) with the lower and upper bound training ECCDFs, for DSF_1 and DSF_3 in States 1, 8, 9 and 10. Evidently, the testing ECCDFs tend to fall outside these bounds when and where structural change is present

(States 8, 9 and 10 at DOF3), otherwise remain inside the bounds for all the other cases where damage is not present. In addition, while in States 8 and 9 the training ECCDFs of DSF3 shift to the right of the training bounds (indicating damage), in State 10 they shift to the left (validating a retrofitting operation). The fact that the testing ECCDFs at non-damaged locations fall within the lower and upper bound training ECCDFs is useful, since it is as important to be able to identify an undamaged structure as undamaged (reduced false alarms), as it is to be able to classify a damaged structure as damaged (reduced false safety). (False alarms will lead to economic losses from unnecessary suspension of operations, while false safety may even lead to structural collapse and loss of life; both will result in a decreased confidence in the SHM system [6].) Within a deterministic framework, a value of the SPDSF higher than 0 would be considered indicative of damage, as only one reference (healthy) structure would be considered. On the contrary, the initial training phase performed in the currently proposed approach enables us to set a reasonable range of values of d, within which a non-zero d can be considered as due to the influence of external factors, e.g. temperature, traffic, wind, etc.

4.2 Existence of change in the state of the system

To quantitatively detect the existence of change in stiffness at a location in the structure under unknown conditions (testing stage), one would need to compute some measure of mismatch (or agreement) between the testing ECCDF and the lower and upper bounds of the training ECCDFs. For this purpose, we compute the measure:

$$\mathcal{P} = F_{\mathcal{T}}(d \mathrel{\widehat{=}} \mathcal{L}_{97.5}) - F_{\mathcal{T}}(d \mathrel{\widehat{=}} \mathcal{U}_{2.5}) \tag{4.1}$$

where $\mathcal{L}$, $\mathcal{U}$ and $F_{\mathcal{T}}$ (or $\mathcal{T}$) denote respectively the lower bound training, upper bound training and testing (from a single test) ECCDFs. The value $d \mathrel{\widehat{=}} \mathcal{L}_{97.5}$ is the d corresponding to the 97.5 percentile of $\mathcal{L}$, while $d \mathrel{\widehat{=}} \mathcal{U}_{2.5}$ is the d corresponding to the 2.5 percentile of $\mathcal{U}$. Then, $F_{\mathcal{T}}(d \mathrel{\widehat{=}} \mathcal{L}_{97.5})$ represents the percentile in $F_{\mathcal{T}}$ corresponding to $d \mathrel{\widehat{=}} \mathcal{L}_{97.5}$, and $F_{\mathcal{T}}(d \mathrel{\widehat{=}} \mathcal{U}_{2.5})$ represents the

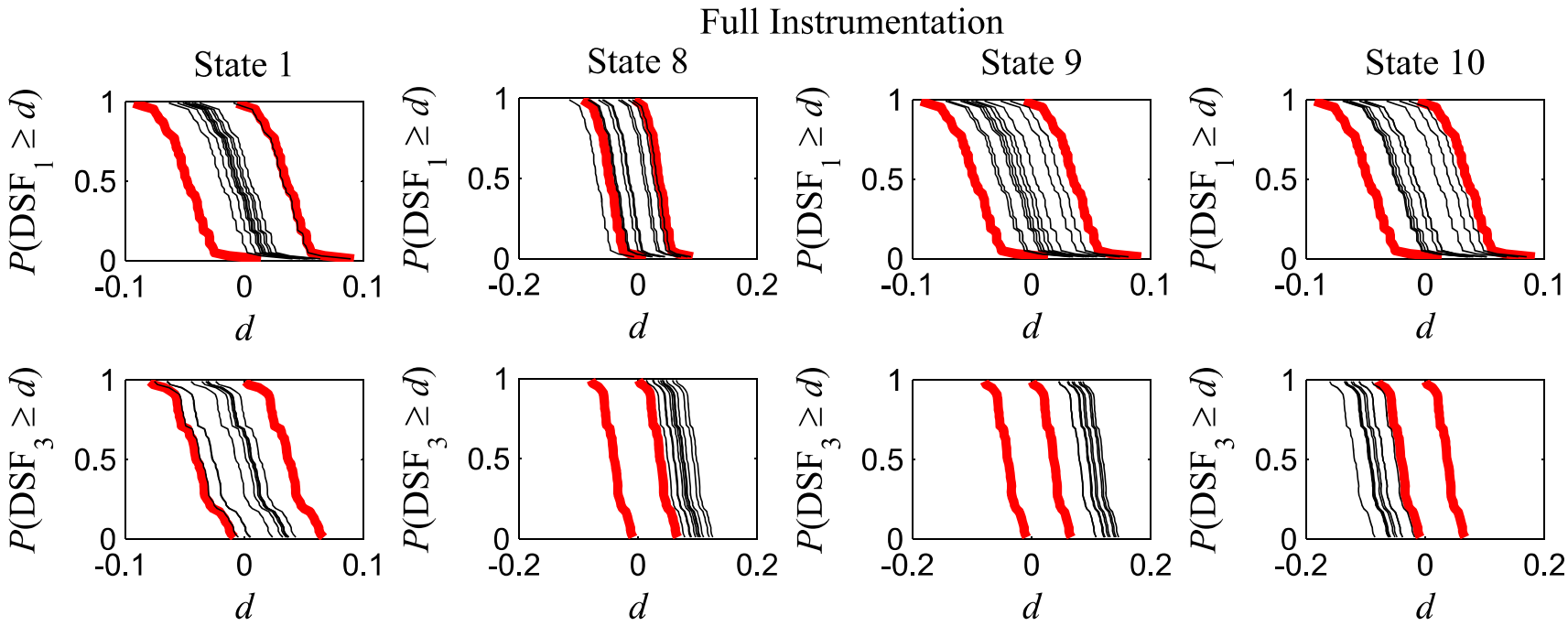

Figure 4.3: ECCDFs of SPDSFs at DOFs 1 and 3, in States 1, 8, 9 and 10, for the full instrumentation scenario. (The thick red curves are the lower and upper bound ECCDFs from training data, while the ensemble of thin black curves are the ECCDFs from testing data; each black curve corresponds to a different test.) In states 8, 9 and 10, the testing ECCDFs for DOF 3 lie outside the region defined by the lower and upper bound training ECCDFs.

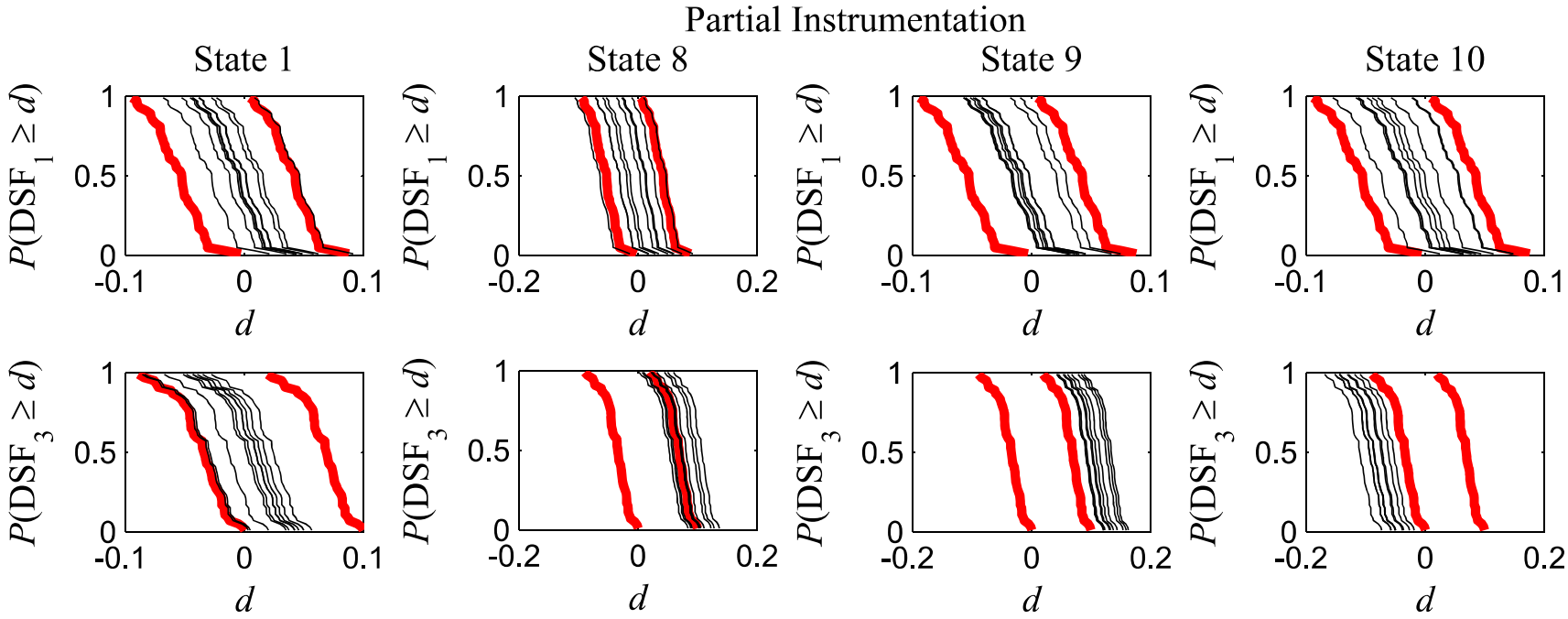

Figure 4.4: ECCDFs of SPDSFs at DOFs 1 and 3, in States 1, 8, 9 and 10, for the partial instrumentation scenario. (The thick red curves are the lower and upper bound ECCDFs from training data, while the ensemble of thin black curves are the ECCDFs from testing data; each black curve corresponds to a different test.) In states 8, 9 and 10, the testing ECCDFs for DOF 3 lie outside the region defined by the lower and upper bound training ECCDFs.

percentile in $F_{\mathcal{T}}$ corresponding to $d \mathrel{\widehat{=}} \mathcal{U}_{2.5}$. This $\mathcal{P}$ value measures how much the testing ECCDF agrees with (falls within) the zone demarcated by the lower and upper bound training ECCDFs; the lower the $\mathcal{P}$ value the lesser is this agreement and higher is the probability that some form of change (in stiffness) exists at that location. Fig. 4.5 illustrates the $\mathcal{P}$ value computation for change detection at DOF 3 in States 1 (DOF 3 undamaged) and 9 (DOF 3 damaged). From Fig. 4.5, it can be seen that in State 1, for both full and partial instrumentation scenarios, the testing ECCDF, $\mathcal{T}$, falls completely between the training boundaries, $\mathcal{L}$ and $\mathcal{U}$; this condition is associated with a value of $\mathcal{P}$ equal to 1, as $F_{\mathcal{T}}(d \mathrel{\widehat{=}} \mathcal{L}_{97.5})$ is equal to 1, while $F_{\mathcal{T}}(d \mathrel{\widehat{=}} \mathcal{U}_{2.5})$ is equal to 0. On the other hand, the testing ECCDF for State 9 falls outside the training boundaries, resulting in a value of $\mathcal{P}$ less than 1, since $F_{\mathcal{T}}(d \mathrel{\widehat{=}} \mathcal{L}_{97.5})$ is again equal to 1, but $F_{\mathcal{T}}(d \mathrel{\widehat{=}} \mathcal{U}_{2.5})$ is approximately 0.8 for the partial instrumentation case, while exactly equal to 1 for the case of full instrumentation. However, it must be noted that the $\mathcal{P}$ value does not indicate whether the change in stiffness is negative (indicating damage) or positive (indicating retrofitting). Tables 4.2 and 4.3 list, respectively for the full and partial instrumentation scenarios, the mean of the $\mathcal{P}$ values computed from the 10 tests on each of the 10 states; the values at the DOFs with change has been highlighted in bold font. Evidently, the $\mathcal{P}$ values are much higher at undamaged/unretrofitted locations.

The wide separation of the $\mathcal{P}$ values, between locations with change (damage or retrofitting) and no change, highlights the potential of the present analysis in meeting both the requirements of a useful classification tool, i.e. classifying unchanged as unchanged and changed as changed. In general, a threshold will need to be selected to define a boundary between changed and unchanged in terms of $\mathcal{P}$. Here we select the threshold $\mathcal{P}_{\text{TH}} = 0.95$, with $\mathcal{P} < \mathcal{P}_{\text{TH}}$ indicating the existence of change in the location under consideration. With this threshold and criterion, we perform the change existence assessment task, for each of the testing cases; Tables 4.4 and 4.5 present the results of this analysis, respectively for the full and partial instrumentation scenarios, with a value of $x/10$ denoting that an existence of change has been detected based on the extracted features in x tests out of the 10 tests. These results show a satisfactory performance of this method, with only 4% $(44/1110)$ misclassification of unchanged as changed and no misclassifications of

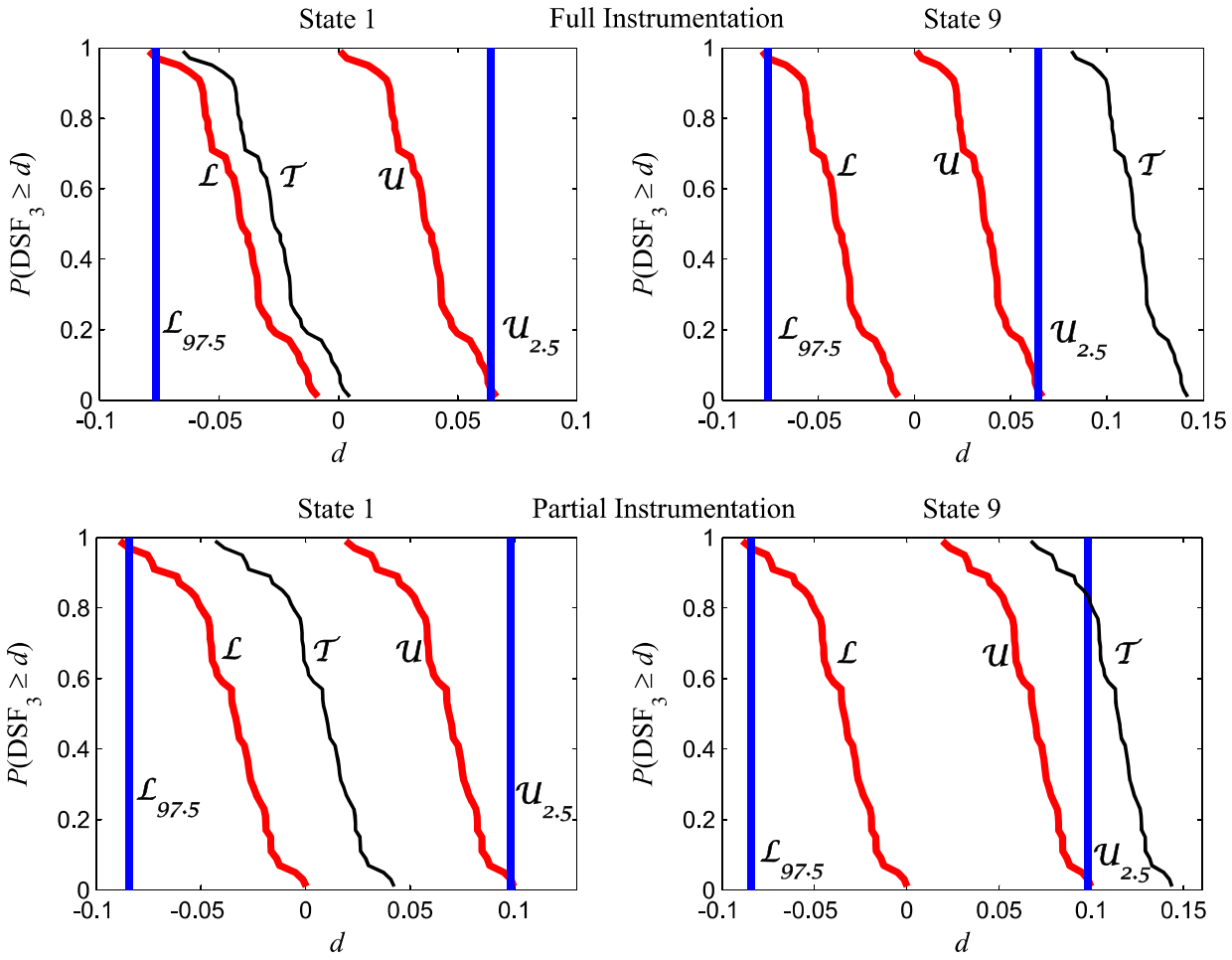

Figure 4.5: Calculation of $\mathcal{P}$ values for SPDSFs of DOF 3, using testing ECCDFs from single tests, in States 1 and 9: $\mathcal{P} = F_{\mathcal{T}}(d \mathrel{\widehat{=}} \mathcal{L}_{97.5}) - F_{\mathcal{T}}(d \mathrel{\widehat{=}} \mathcal{U}_{2.5})$. ($\mathcal{L}$: lower bound training ECCDF $\mathcal{L}$; $\mathcal{U}$: upper bound training ECCDF $\mathcal{U}$; $\mathcal{T}$: sample testing ECCDF $F_{\mathcal{T}}$ (from single test); $\mathcal{L}_{97.5}$: 97.5 percentile of $\mathcal{L}$; $\mathcal{U}_{2.5}$: 2.5 percentile of $\mathcal{U}$.)

Table 4.2: Mean $\mathcal{P}$ values (change locations in bold) for full instrumentation.

DOFs	States									
	1	2	3	4	5	6	7	8	9	10
1	0.98	0.97	0.98	0.98	0.98	**0.10**	0.98	0.95	0.98	0.97
2	0.98	0.98	0.97	0.98	0.97	0.94	**0.19**	**0.11**	**0.02**	**0.18**
3	0.98	0.97	0.98	0.96	0.97	0.94	0.98	**0.31**	**0.02**	**0.35**
4	0.97	0.98	0.98	0.98	0.98	0.96	0.98	0.98	0.96	0.98
5	0.98	0.98	0.96	0.98	0.95	0.98	0.96	0.91	0.98	0.97
6	0.98	0.98	0.97	0.98	0.95	0.98	0.98	0.92	0.97	0.98
7	0.98	0.97	0.97	0.97	0.97	0.95	0.98	0.97	0.90	0.98
8	0.98	0.96	0.98	0.98	0.98	0.98	**0.20**	0.97	0.98	0.98
9	0.98	0.98	0.98	0.98	0.98	0.98	0.98	0.98	0.98	0.98
10	0.98	0.97	0.98	0.98	0.98	0.97	0.98	0.98	0.96	0.98
11	0.98	0.97	0.97	0.98	0.97	0.98	0.98	0.94	0.97	0.97
12	0.98	0.98	0.98	0.98	0.92	0.98	0.98	0.95	0.98	0.98

Table 4.3: Mean $\mathcal{P}$ values (change locations in bold) for partial instrumentation.

DOFs	States									
	1	2	3	4	5	6	7	8	9	10
1	0.98	0.98	0.98	0.98	0.98	**0.16**	0.98	0.97	0.98	0.98
3	0.98	0.98	0.98	0.97	0.98	0.97	0.98	**0.81**	**0.34**	**0.50**
5	0.98	0.98	0.98	0.98	0.98	0.98	0.98	0.98	0.98	0.98
6	0.98	0.98	0.97	0.98	0.98	0.98	0.98	0.95	0.98	0.98
7	0.98	0.98	0.98	0.98	0.98	0.98	0.98	0.98	0.91	0.98
8	0.98	0.98	0.98	0.98	0.98	0.98	**0.38**	0.98	0.98	0.98
10	0.98	0.98	0.98	0.98	0.98	0.98	0.98	0.98	0.98	0.98
12	0.98	0.98	0.98	0.97	0.94	0.97	0.98	0.97	0.98	0.98

Table 4.4: Change existence detection using $\mathcal{P}$ values with $\mathcal{P}_{\text{th}} = 0.95$ ($\mathcal{P} < \mathcal{P}_{\text{th}} \Rightarrow$ change) for full instrumentation.

DOFs	States									
	1	2	3	4	5	6	7	8	9	10
1	0/10	0/10	0/10	0/10	0/10	**10/10**	0/10	1/10	0/10	0/10
2	0/10	0/10	1/10	0/10	1/10	1/10	**10/10**	**10/10**	**10/10**	**10/10**
3	0/10	1/10	0/10	1/10	1/10	1/10	0/10	**10/10**	**10/10**	**10/10**
4	1/10	0/10	0/10	0/10	0/10	2/10	0/10	0/10	1/10	0/10
5	0/10	0/10	1/10	0/10	2/10	0/10	1/10	4/10	0/10	1/10
6	0/10	0/10	1/10	0/10	2/10	0/10	0/10	3/10	0/10	0/10
7	0/10	1/10	0/10	1/10	0/10	1/10	0/10	0/10	1/10	0/10
8	0/10	1/10	0/10	0/10	0/10	0/10	**10/10**	2/10	0/10	0/10
9	0/10	0/10	0/10	0/10	0/10	0/10	0/10	0/10	0/10	0/10
10	0/10	1/10	0/10	0/10	0/10	1/10	0/10	0/10	1/10	0/10
11	0/10	1/10	0/10	0/10	0/10	0/10	0/10	2/10	0/10	1/10
12	0/10	0/10	0/10	0/10	2/10	0/10	0/10	1/10	0/10	0/10

Table 4.5: Change existence detection using $\mathcal{P}$ values with $\mathcal{P}_{\text{th}} = 0.95$ ($\mathcal{P} < \mathcal{P}_{\text{th}} \Rightarrow$ change) for partial instrumentation.

DOFs	States									
	1	2	3	4	5	6	7	8	9	10
1	1/10	0/10	0/10	0/10	0/10	**10/10**	0/10	2/10	0/10	0/10
3	0/10	0/10	0/10	1/10	0/10	1/10	0/10	**7/10**	**10/10**	**10/10**
5	1/10	0/10	1/10	0/10	0/10	0/10	0/10	0/10	0/10	0/10
6	0/10	0/10	2/10	0/10	0/10	0/10	0/10	2/10	0/10	0/10
7	0/10	0/10	0/10	0/10	0/10	0/10	0/10	0/10	1/10	0/10
8	0/10	0/10	0/10	0/10	0/10	0/10	**10/10**	0/10	0/10	0/10
10	0/10	0/10	0/10	0/10	0/10	0/10	0/10	0/10	0/10	0/10
12	0/10	0/10	0/10	0/10	1/10	0/10	0/10	1/10	0/10	0/10

changed as unchanged for the full instrumentation scenario, and 1.9% $(14/750)$ misclassification of unchanged as changed and 6% $(3/50)$ misclassifications of changed as unchanged for the partial instrumentation scenario.

With full instrumentation we may also locate the stiffness element(s) that have experience damage or that have undergone retrofitting: in States 8, 9 and 10, DOFs 2 and 3 show the existence of change, and hence the stiffness k_3 has changed; similarly in States 7 k_{16} has changed, while in State 6, only DOF 1 shows the existence of change, and hence k_1 has changed. However, for the partial instrumentation scenario, such an element level change detection will *in general* not

be possible: in States 8, 9 and 10, DOF 3 shows the existence of change, but since DOFs 2, 4 and 9 are unmeasured, any/all of the stiffnesses k_3, k_4 and k_{17} may have changed; similarly in State 7 either/both k_{10} and k_{16} may have changed, while in State 6 either/both k_1 and k_2 may have changed. We say *in general* because, in case all of the neighbouring DOFs of a given DOF is measured, then it will be possible to detect the individual stiffness element(s) with change, for the stiffness elements connecting to that given DOF; e.g. if the damaged elements were amongst $\{k_8, k_9, k_{15}, k_6, k_7, k_{20}\}$, then it would have been possible to detect them even in the partial instrumentation case. An alternative in partial instrumentation scenarios will be to estimate the mode shape components at the unmeasured DOFs using, e.g. additional model topology requirements [3, 4], at the cost of introducing more modeling assumptions into the solution.

4.3 Existence and type of change: Localized stiffness reduction vs. increase

While the $\mathcal{P}$ value does a two-class classification (changed vs. unchanged), it does not differentiate between damage induced (stiffness decrease) and retrofitting induced (stiffness increase) changes. It may be better however to instead perform, if possible, a three-class classification: unchanged vs. damaged vs. retrofitted. This may be important especially in verification of retrofitting operations, where an intentional interference into the structural system has the possibility of unintentional introduction of structural damage. We explore here such an alternative classification exercise using the Łukaszyk–Karmowski metric [19], which compares two probability distributions (density functions) as:

$$\mathcal{D}_{X,Y} = \int_{-\infty}^{\infty}\int_{-\infty}^{\infty} |x-y| f_X(x) g_Y(y) \mathrm{d}x\mathrm{d}y \tag{4.2}$$

where $f_X(x)$ and $g_Y(y)$ are the probability density functions of the random variables x and y. $\mathcal{D}_{X,Y}$ is not a distance metric in the strict sense as it, in general, does not satisfy the identity of indiscernibles: $\mathcal{D}_{X,X} \neq 0$ unless x (and $y = x$) have a Dirac delta distribution, i.e. $x = y$ is actually

one *exact* value. The generally non-zero value of $\mathcal{D}_{X,X}$ may be seen as a reflection of inevitable experimental error [19], since even for the same parameter, different sets of experiments will lead to different sets of measured values. The most useful property of the Łukaszyk–Karmowski metric from our perspective is that it *satisfies the triangle inequality as an equality*, i.e. $\mathcal{D}_{X,Z} = \mathcal{D}_{X,Y} + \mathcal{D}_{Y,Z}$. This property may be exploited to solve our three-class classification problem as follows: let $f_{\mathcal{L}}$, $f_{\mathcal{U}}$ and $f_{\mathcal{T}}$ be the *empirical probability density functions* (epdfs) corresponding respectively to the lower bound training, upper bound training and testing ECCDFs. Then:

$$\begin{aligned}
&\mathcal{D}_{\mathcal{LU}} \approx \mathcal{D}_{\mathcal{LT}} + \mathcal{D}_{\mathcal{UT}} \text{ i.e. } \frac{\mathcal{D}_{\mathcal{LU}}}{\mathcal{D}_{\mathcal{LT}} + \mathcal{D}_{\mathcal{UT}}} \approx 1 \Rightarrow \text{ no stiffness change in testing state} \\
&\mathcal{D}_{\mathcal{LT}} \approx \mathcal{D}_{\mathcal{LU}} + \mathcal{D}_{\mathcal{UT}} \text{ i.e. } \frac{\mathcal{D}_{\mathcal{LT}}}{\mathcal{D}_{\mathcal{LU}} + \mathcal{D}_{\mathcal{UT}}} \approx 1 \Rightarrow \text{ stiffness decrease (damage) in testing state} \\
&\mathcal{D}_{\mathcal{UT}} \approx \mathcal{D}_{\mathcal{LU}} + \mathcal{D}_{\mathcal{LT}} \text{ i.e. } \frac{\mathcal{D}_{\mathcal{UT}}}{\mathcal{D}_{\mathcal{LU}} + \mathcal{D}_{\mathcal{LT}}} \approx 1 \Rightarrow \text{ stiffness increase (retrofit) in testing state}
\end{aligned} \tag{4.3}$$

In Eq. (4.3) we use "$\approx$" instead of "$=$" to account for numerical errors introduced in the computation of the epdfs from the ECCDFs, and in the 2-D numerical integration necessary to compute the Łukaszyk–Karmowski metrics from the epdfs. Here, we compute the epdfs as histograms from the decreases in the ECCDFs at different d's; Fig. 4.6 shows such histogram plots for the DSFs at DOF 3 in States 1 (DOF 3 undamaged) and 9 (DOF 3 damaged). The testing epdfs are constructed, for each state, using the mean of the DSFs estimated in the 10 tests. The necessary numerical integrations are performed using the trapezoidal rule in 2-D. Tables 4.6 to 4.8 and 4.9 to 4.11 lists, respectively for the full and partial instrumentation scenarios, the values of the three ratios of the computed Łukaszyk–Karmowski metrics given in Eq. (4.3); the values at the stiffness change locations are highlighted in bold font. Evidently, the first ratio, $\mathcal{D}_{\mathcal{LU}}/(\mathcal{D}_{\mathcal{LT}} + \mathcal{D}_{\mathcal{UT}})$, correctly indicates the presence of change (stiffness increase or decrease) at a DOF by taking values much lesser than 1; the second ratio, $\mathcal{D}_{\mathcal{LT}}/(\mathcal{D}_{\mathcal{LU}} + \mathcal{D}_{\mathcal{UT}})$, indicates the presence of damage induced change (stiffness decrease) by taking values close to 1; while the third ratio, $\mathcal{D}_{\mathcal{UT}}/(\mathcal{D}_{\mathcal{LU}} + \mathcal{D}_{\mathcal{LT}})$, indicates the presence of retrofitting induced change (stiffness increase) by taking values close to 1.

As in the change detection using $\mathcal{P}$ values, using the Łukaszyk–Karmowski metric ratios too

we may locate the individual stiffness element(s) with damage/retrofit in the full instrumentation scenario, but, in general, only a neighbourhood consisting of a set of possible stiffness element(s) with damage/retrofit in the partial instrumentation scenario.

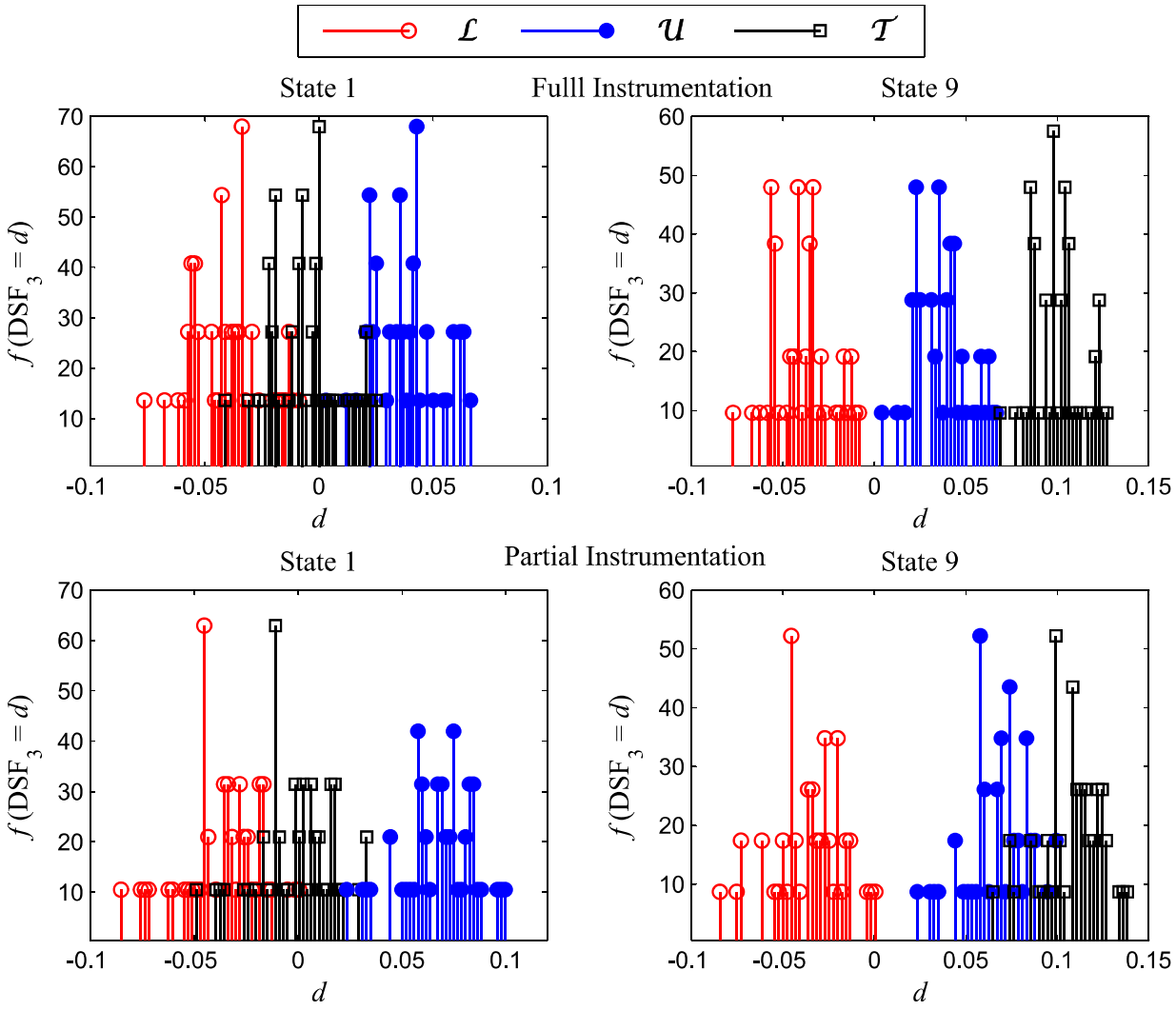

Figure 4.6: Approximate empirical probability density functions (epdf), computed as histograms from corresponding ECCDFs, for SPDSFs of DOF 3 in States 1 and 9. ($\mathcal{L}$: lower bound training epdf $f_{\mathcal{L}}$; $\mathcal{U}$: upper bound training epdf $f_{\mathcal{U}}$; $\mathcal{T}$: mean (of 10 tests) testing epdf $f_{\mathcal{T}}$.)

Table 4.6: Ratio $\mathcal{D}_{\mathcal{LU}}/(\mathcal{D}_{\mathcal{LT}} + \mathcal{D}_{\mathcal{UT}})$ ($\approx 1 \Rightarrow$ no stiffness change) for full instrumentation.

DOFs	States									
	1	2	3	4	5	6	7	8	9	10
1	0.97	0.96	0.97	0.96	0.97	**0.42**	0.97	0.97	0.97	0.97
2	0.98	0.97	0.98	0.97	0.97	0.97	**0.50**	**0.45**	**0.36**	**0.41**
3	0.98	0.96	0.98	0.97	0.97	0.98	0.98	**0.52**	**0.39**	**0.46**
4	0.96	0.96	0.95	0.96	0.96	0.96	0.96	0.95	0.96	0.96
5	0.97	0.96	0.95	0.97	0.95	0.97	0.96	0.89	0.97	0.97
6	0.95	0.95	0.93	0.94	0.95	0.94	0.95	0.93	0.95	0.95
7	0.97	0.97	0.95	0.93	0.97	0.95	0.97	0.97	0.97	0.97
8	0.93	0.94	0.93	0.94	0.94	0.94	**0.44**	0.93	0.95	0.94
9	0.97	0.98	0.98	0.98	0.97	0.98	0.98	0.98	0.98	0.98
10	0.96	0.96	0.95	0.96	0.96	0.93	0.96	0.96	0.95	0.96
11	0.96	0.95	0.96	0.95	0.96	0.96	0.96	0.94	0.96	0.96
12	0.96	0.96	0.96	0.93	0.92	0.96	0.96	0.94	0.96	0.95

Table 4.7: Ratio $\mathcal{D}_{\mathcal{LT}}/(\mathcal{D}_{\mathcal{LU}} + \mathcal{D}_{\mathcal{UT}})$ ($\approx 1 \Rightarrow$ stiffness decrease/damage) for full instrumentation.

DOFs	States									
	1	2	3	4	5	6	7	8	9	10
1	0.39	0.43	0.31	0.24	0.32	**0.99**	0.32	0.30	0.35	0.35
2	0.36	0.46	0.31	0.46	0.50	0.45	**0.99**	**0.99**	**0.99**	0.27
3	0.30	0.54	0.31	0.49	0.48	0.41	0.39	**0.99**	**0.99**	0.23
4	0.32	0.35	0.26	0.33	0.32	0.40	0.34	0.27	0.40	0.31
5	0.33	0.43	0.22	0.31	0.24	0.34	0.26	0.16	0.41	0.30
6	0.36	0.37	0.24	0.28	0.33	0.27	0.30	0.50	0.35	0.37
7	0.40	0.43	0.56	0.64	0.46	0.57	0.45	0.43	0.41	0.46
8	0.47	0.42	0.26	0.43	0.29	0.35	**0.99**	0.27	0.36	0.30
9	0.45	0.37	0.38	0.42	0.26	0.41	0.33	0.44	0.39	0.29
10	0.34	0.32	0.25	0.34	0.28	0.22	0.31	0.43	0.25	0.29
11	0.30	0.27	0.30	0.47	0.28	0.30	0.28	0.51	0.41	0.30
12	0.41	0.42	0.31	0.56	0.20	0.39	0.33	0.22	0.41	0.48

Table 4.8: Ratio $\mathcal{D}_{\mathcal{UT}}/(\mathcal{D}_{\mathcal{LU}} + \mathcal{D}_{\mathcal{LT}})$ ($\approx 1 \Rightarrow$ stiffness increase/retrofit) for full instrumentation.

DOFs	States									
	1	2	3	4	5	6	7	8	9	10
1	0.29	0.26	0.37	0.46	0.36	0.26	0.36	0.39	0.33	0.33
2	0.31	0.24	0.37	0.24	0.21	0.25	0.21	0.24	0.31	**0.99**
3	0.38	0.19	0.37	0.22	0.23	0.28	0.29	0.19	0.29	**0.99**
4	0.37	0.34	0.44	0.35	0.37	0.29	0.35	0.42	0.29	0.38
5	0.35	0.27	0.49	0.37	0.47	0.34	0.43	0.64	0.28	0.39
6	0.33	0.32	0.48	0.42	0.36	0.43	0.39	0.23	0.34	0.32
7	0.28	0.26	0.18	0.15	0.24	0.18	0.25	0.26	0.27	0.24
8	0.25	0.28	0.45	0.28	0.41	0.35	0.24	0.44	0.33	0.39
9	0.25	0.31	0.30	0.26	0.43	0.27	0.35	0.25	0.29	0.39
10	0.35	0.36	0.45	0.34	0.42	0.52	0.37	0.27	0.46	0.40
11	0.39	0.43	0.39	0.24	0.41	0.38	0.41	0.22	0.28	0.39
12	0.28	0.27	0.37	0.19	0.55	0.29	0.36	0.50	0.28	0.23

Table 4.9: Ratio $\mathcal{D}_{\mathcal{LU}}/(\mathcal{D}_{\mathcal{LT}} + \mathcal{D}_{\mathcal{UT}})$ ($\approx 1 \Rightarrow$ no stiffness change) for partial instrumentation.

DOFs	States									
	1	2	3	4	5	6	7	8	9	10
1	0.98	0.98	0.98	0.98	0.98	**0.46**	0.98	0.98	0.98	0.98
3	0.97	0.99	0.97	0.99	0.99	0.98	0.98	**0.80**	**0.57**	**0.51**
5	0.98	0.98	0.97	0.98	0.98	0.98	0.97	0.96	0.97	0.98
6	0.96	0.96	0.93	0.95	0.95	0.95	0.96	0.96	0.96	0.96
7	0.98	0.97	0.96	0.95	0.97	0.96	0.98	0.97	0.98	0.98
8	0.95	0.97	0.97	0.97	0.97	0.97	**0.54**	0.97	0.97	0.97
10	0.98	0.98	0.96	0.98	0.97	0.95	0.97	0.98	0.97	0.96
12	0.94	0.94	0.95	0.89	0.92	0.93	0.95	0.92	0.94	0.92

Table 4.10: Ratio $\mathcal{D}_{\mathcal{LT}}/(\mathcal{D}_{\mathcal{LU}} + \mathcal{D}_{\mathcal{UT}})$ ($\approx 1 \Rightarrow$ stiffness decrease/damage) for partial instrumentation.

DOFs	States									
	1	2	3	4	5	6	7	8	9	10
1	0.41	0.42	0.35	0.29	0.35	**0.99**	0.37	0.34	0.36	0.36
3	0.22	0.37	0.20	0.31	0.36	0.27	0.28	**0.89**	**0.99**	0.20
5	0.39	0.38	0.26	0.38	0.34	0.39	0.30	0.23	0.42	0.32
6	0.32	0.30	0.22	0.26	0.26	0.26	0.27	0.44	0.34	0.30
7	0.32	0.40	0.49	0.56	0.41	0.53	0.38	0.39	0.35	0.35
8	0.50	0.37	0.29	0.45	0.34	0.36	**0.98**	0.35	0.38	0.30
10	0.26	0.26	0.19	0.26	0.23	0.18	0.25	0.30	0.22	0.21
12	0.45	0.40	0.35	0.59	0.25	0.46	0.35	0.26	0.45	0.49

Table 4.11: Ratio $\mathcal{D}_{\mathcal{UT}}/(\mathcal{D}_{\mathcal{LU}} + \mathcal{D}_{\mathcal{LT}})$ ($\approx 1 \Rightarrow$ stiffness increase/retrofit) for partial instrumentation.

DOFs	States									
	1	2	3	4	5	6	7	8	9	10
1	0.27	0.27	0.32	0.39	0.32	0.23	0.31	0.33	0.32	0.32
3	0.49	0.31	0.52	0.36	0.32	0.41	0.40	0.09	0.17	**0.99**
5	0.29	0.30	0.43	0.30	0.33	0.29	0.39	0.47	0.27	0.36
6	0.37	0.39	0.52	0.44	0.44	0.44	0.42	0.26	0.35	0.39
7	0.36	0.29	0.22	0.18	0.27	0.20	0.30	0.30	0.33	0.33
8	0.21	0.31	0.40	0.25	0.33	0.32	0.18	0.33	0.31	0.39
10	0.43	0.43	0.53	0.43	0.47	0.56	0.44	0.38	0.49	0.51
12	0.26	0.30	0.34	0.19	0.47	0.25	0.34	0.46	0.26	0.24

4.4 Severity of change

Once a location with potential stiffness change in the testing state has been identified using the $\mathcal{P}$ values or the Łukaszyk–Karmowski metric ratios, the testing ECCDF ($F_{\mathcal{T}}$) can be further used with the lower ($\mathcal{L}$) and upper ($\mathcal{U}$) bound training ECCDFs to quantify the severity of the change in a probabilistic sense. This may be achieved by first selecting two values of d corresponding to some percentiles of $\mathcal{L}$ and $\mathcal{U}$; let these two values be $d_{\gamma_{\mathcal{L}}}$ and $d_{\gamma_{\mathcal{U}}}$, corresponding respectively to the $\gamma_{\mathcal{L}}$th percentile of $\mathcal{L}$ and $\gamma_{\mathcal{U}}$th percentile of $\mathcal{U}$. Also, let $d_{\gamma_{\mathcal{T}}}$ be the d corresponding to any $\gamma_{\mathcal{T}}$th percentile of $F_{\mathcal{T}}$. Then, the testing ECCDF can be adjusted to account for the training variability to get two new ECCDFs depicting a lower and upper bound damage probability vs. damage severity as:

$$\left.\begin{aligned} F_D = P(D \geq d) = \gamma_{\mathcal{T}}, \qquad & \text{where } d = d_{\gamma_{\mathcal{T}}} - d_{\gamma_{\mathcal{L}}} \\ F_D = P(D \geq d) = \gamma_{\mathcal{T}}, \qquad & \text{where } d = d_{\gamma_{\mathcal{T}}} - d_{\gamma_{\mathcal{U}}} \end{aligned}\right\} \quad \forall\, \gamma_{\mathcal{T}} \in [0;1] \tag{4.4}$$

resulting in a probability box model of the uncertainty in damage severity. Figs. 4.7 and 4.8 shows such lower and upper bound damage probability vs. damage severity curves, corresponding to $\gamma_{\mathcal{L}} = 0.05$ and $\gamma_{\mathcal{U}} = 0.95$, for DOF3 in States 1 (no damage), 8 (damage), 9 (damage) and 10 (retrofit). Using such curves we can make inferences of the form: (a) for a given damage severity d, the probability that the damage at that location is *at least* d is between $\underline{F_D}$ (a lower bound probability) and $\overline{F_D}$ (a higher bound probability), and (b) for a given damage probability F_D, there is a probability F_D that there exists *at least* between $\underline{d}$ (a lower bound least severity)and $\overline{d}$ (a higher bound least severity) damage at that location. For example, from Fig. 4.7, inferences like the following can be made for DOF 3 in State 9: For the full instrumentation scenario (a) the probability that there is at least 10% damage (stiffness reduction) is between 19% and 77%, and (b) there is a probability of 60% that there exists at least 8.5% to 11% damage; for the partial instrumentation scenario (c) the probability that there is at least 8% damage is between 43% and 96%, and (d) there is a probability of 80% that there is at least 6.3% to 10.7% damage. Similarly, from Fig. 4.8, some possible inferences are: the probability that there is at least 6% damage

(stiffness reduction) in State 8 is (a) between 54% and 96%, given full instrumentation, and (c) between 16% and 90%, given partial instrumentation; there is a probability of 80% that there exists (b) at least 4.8% to 7.3% damage, given full instrumentation, and (d) at least 3.1% to 7.5% damage, given partial instrumentation; the probability that there is at most 10% stiffness increase (retrofit) in State 10 is (e) between 60% and 95%, given full instrumentation, and (g) between 25% and 89%, given partial instrumentation; there is a probability of 60% that there is (f) at most 7.5% to 10% stiffness increase, given full instrumentation, and (h) at most 7.7% to 12% stiffness increase, given partial instrumentation.

From the curves for State 9 (Fig. 4.7), it can be seen that the least damage severity at DOF3 is estimated to be between 8.5% and 11% (full instrumentation), or between 7% and 11.5% (partial instrumentation), with a 60% probability. Also, with full instrumentation, the estimated damage severity ranges between 7.5% (with 80% probability of exceedance, compared to 95th percentile of $F_{\mathcal{U}}$) and 12% (with 20% probability of exceedance, compared to 5th percentile of $F_{\mathcal{L}}$), while for partial instrumentation this estimate ranges from 6.3% to 13.3%. Since all the three flexural links (k_3, k_4 and k_{17}) connected to the lumped mass m_3 have the same undamaged stiffness, assuming no random element stiffness perturbation, the theoretical approximate reduction in the stiffness matrix element $K_{3,3}$ for State 9 (30% reduction in k_3) is 10%. The estimated damage severity from our analysis compares reasonably well with this approximate theoretical estimate. The estimation uncertainty increases slightly in the partial instrumentation scenario, which may be expected owing to less measured information in this scenario. Moreover, the missing measured information for partial instrumentation does not allow us to do an element level damage severity quantification. For example, based on the estimated least reduction, with a 60% probability, in $K_{3,3}$ in State 9, and assuming $k_3 = k_4 = k_{17} = k_0$, we can estimate the severity of reduction, say α, in k_3 as:

$$\frac{3k_0 - (2+\alpha)k_0}{3k_0} \in [0.085, 0.11] \quad \Rightarrow \alpha \in [0.67, 0.745] \tag{4.5}$$

i.e. there is a probability of 60% that the reduction in stiffness k_3 is at least between 67% and

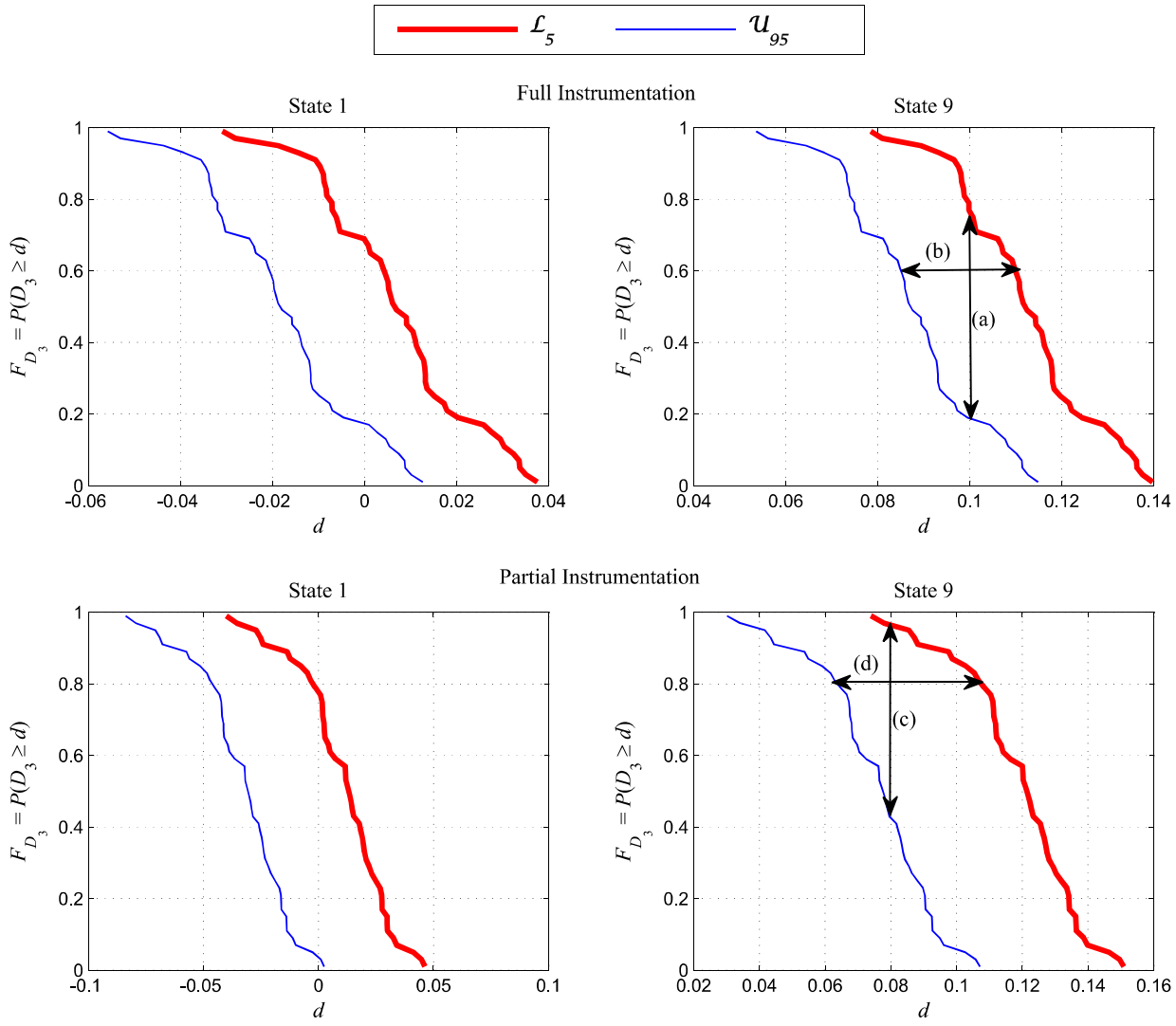

Figure 4.7: *Uncertain* probabilistic description of damage severity, at DOF 3 in States 1 and 9, using lower and upper bound damage probability vs. damage severity curves, obtained by comparing the mean testing ECCDFs with the 95 percentile of the upper bound training ECCDFs ($\mathcal{U}_{95}$) and 5 percentile of the lower bound training ECCDFs ($\mathcal{L}_5$).

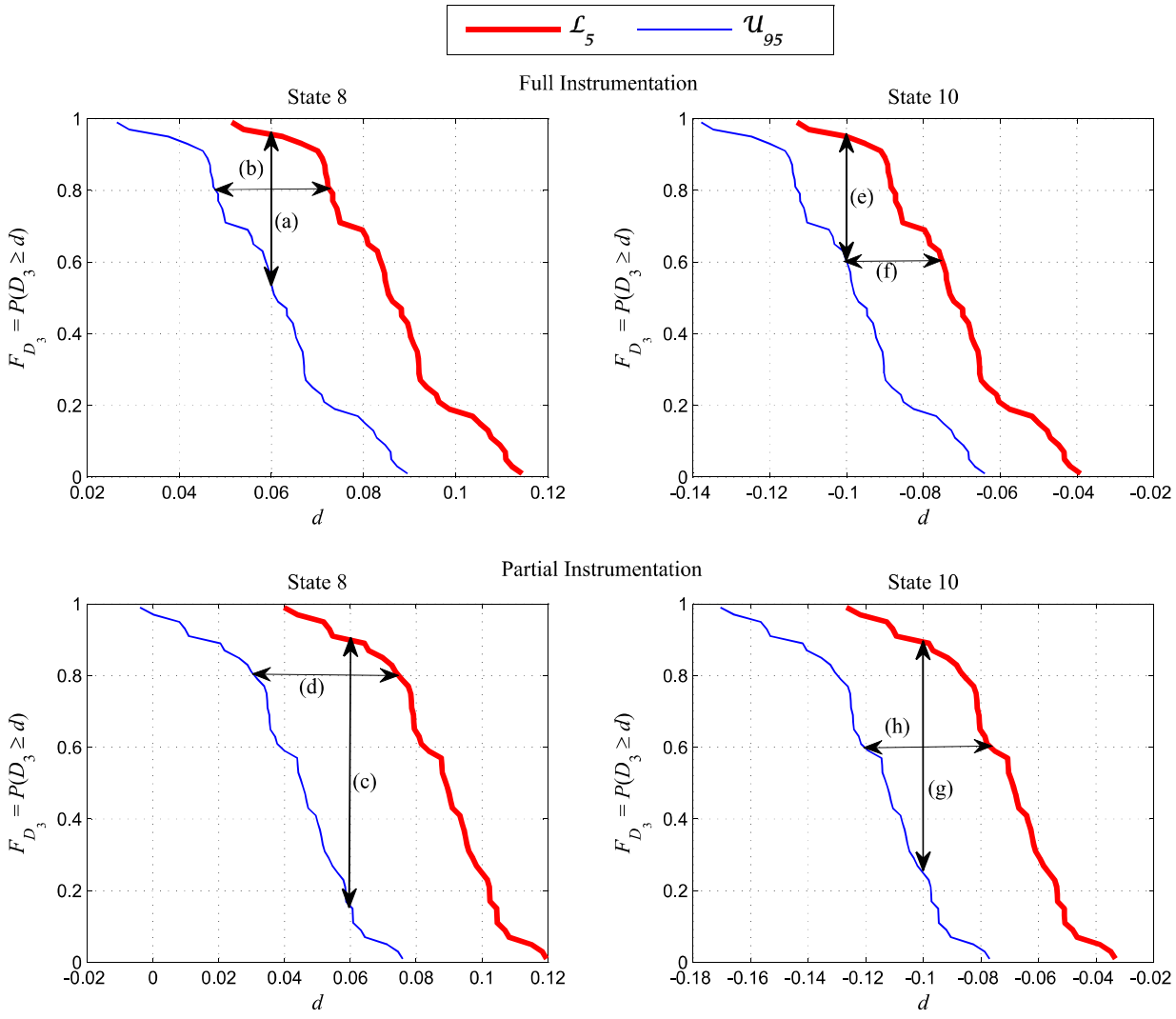

Figure 4.8: *Uncertain* probabilistic description of damage severity at DOF 3 in States 8 and 10, using lower and upper bound damage probability vs. damage severity curves, obtained by comparing the mean testing ECCDFs with the 95 percentile of the upper bound training ECCDFs ($\mathcal{U}_{95}$) and 5 percentile of the lower bound training ECCDFs ($\mathcal{L}_5$).

74.5%. The calculation in Eq. (4.5) is possible because of full instrumentation, which allows us to locate the individual damaged element as k_3, as discussed at the end of the sections on change existence detection. Since with partial instrumentation we will not be able to identify the individual element k_3 as damaged, we will not be able to quantify the element level damage severity accurately; in such a case the estimated element level damage will range from mild and distributed (all of k_3, k_4 and k_{17} damaged) to severe and localized (either of k_3, k_4 or k_{17} damaged). Discussions and calculations similar to this paragraph on State 9 may also be done for the damage severities in other damage states, e.g. State 1 (healthy, low damage severity) from Fig. 4.7, and States 8 (damaged, but lower severity than State 9) and 10 (retrofitted, negative damage severity) from Fig. 4.8.

The two level uncertainty in the damage severity expressed through the two ECCDFs in Eq. (4.4) may be interpreted in the following way: (a) the uncertainty (probability) of damage severity given by a single ECCDF will include the effects of measurement noise, input variability, and also the environmental/opetational variability in the training (healthy) state, while (b) the range of possible values the damage probability may take will include the effect of *unknown environmental/opetational conditions in the testing state*. This interpretation is a result of the definition of the DSF in Section 2 and the computation of the ECCDFs in Section 3. Based on these, using the terminology of Section 2, each individual ECCDF depicts the variability of the *baseline* state, while the possible range of such ECCDFs (denoted by the lower and upper bounds) depict the variability of the *alternative* state. While the alternative state's variability is taken into account in the training stage by including data from different environmental/opetational conditions in the set Y_V of modal parameters, in the testing stage, with a single test, we can assume a stationary environmental/operational conditions (no variability). This stationary environmental/operational condition is however unknown to us. Hence, instead of comparing the testing ECCDF against only one training ECCDF, it may be better to compare it against the entire range of possible training ECCDFs, or alternatively to the lower and upper bound training ECCDFs as done here, to take into account our lack of knowledge of the testing environmental/operational conditions. Such a

comparison will account for our lack of knowledge by treating the testing data to be coming from different (hypothetical) environmental/operational conditions.

5. Experimental Application

Although the example considered in the numerical validation is on a bridge deck, the developed methodology may be applied to any other type of structural system as well. While the project is primarily targeted towards SHM of bridges, data from damaged real bridges are difficult to obtain. However, future experiments using a laboratory scale bridge system are currently in the planning stage at the Carleton Laboratory of Columbia University. In order to demonstrate the robustness of the proposed methodology when applied to experimental data, in this section, we present the results obtained using the data collected from a four story steel frame subjected to base excitation using the shake table facility available at the Carleton Laboratory of Columbia University (Figure 5.1).

The frame has an inter-story height of 533 mm, floor plate dimensions of 610 x 457 x 12.7 mm, and it is diagonally braced in one direction (North-South direction), from here onwards denoted as the strong direction, as opposed to the perpendicular direction (East-West direction), referred to as the weak direction. The columns and the diagonal braces have cross-sectional dimensions of 50.8 x 9.5 mm and 50.8 x 6.4 mm, respectively. All the structural connections are bolted using connection plates and angles. The frame is excited along the weak direction of bending. The base excitation is provided using the 1.5 x 1.5 m platform uniaxial hydraulic shaking table facility available at the Carleton Laboratory of Columbia University, New York. The frame is mounted on the table and the structure-table connection is sufficiently bolted to reproduce a fixed-base behavior. In the discussion herein, we use the structural acceleration at the centroids of the floors, indicated as $\ddot{u}_i$ in Figure 5.2, for $i = 1, , 4$. Using the assumption of rigid floors and the coincidence of floor centers of mass and centroids, the frame is modeled as a 1-D 4-DOF system. Six different types of input

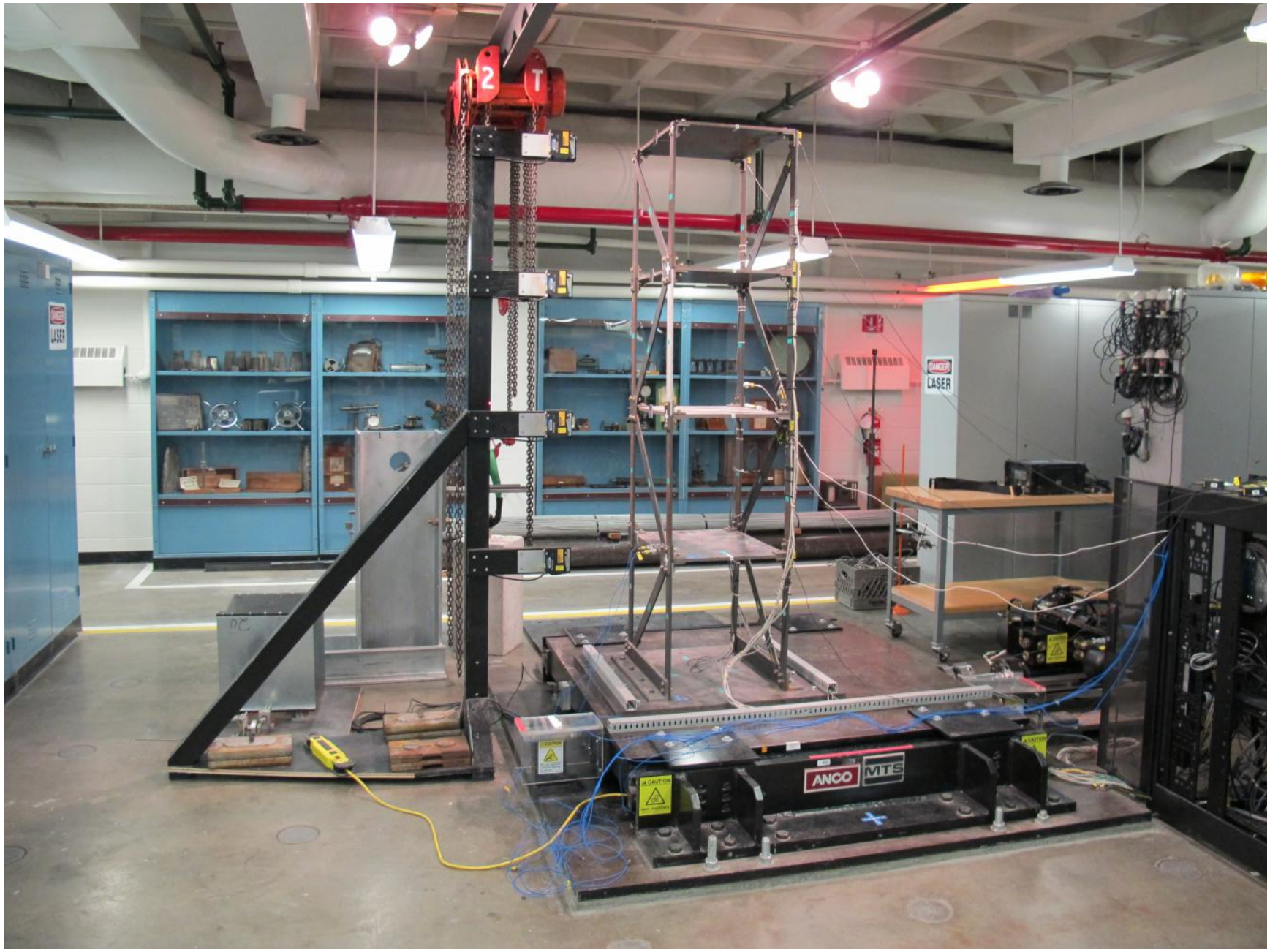

Figure 5.1: Four-story steel frame subjected to base excitation through the shake table available at the Carleton Laboratory of Columbia University.

Table 5.1: Different states of the steel frame considered for the experimental application.

State	**Condition**	**Description**	**Affected DOFs**	**Stiffness Reduction at affected DOFs**
U1	Undamaged	Baseline Condition	-	-
U2	Undamaged	40% mass addition to 3^{rd} floor	-	-
D1	Damaged	15% stiffness reduction at 3^{rd} floor	2 and 3	7.5% at DOFs 2 and 3
D2	Damaged	30% stiffness reduction at 3^{rd} floor	2 and 3	15% at DOFs 2 and 3
D3	Damaged	60% stiffness reduction at 3^{rd} floor	2 and 3	30% at DOFs 2 and 3
D4	Damaged	15% stiffness reduction at 2^{nd} and 3^{rd} floors	1,2 and 3	7.5% at DOFs 1 and 3, 15% at DOF 2

ground motions (band limited white noise, EC8, El Centro, Hachinohe, Kobe and Northridge) are applied to the table. For this application, the OKID/ERA [28] algorithm is employed to identify the modal properties of the frame, using the measured acceleration responses of the floors as outputs and of the table as input.

To assess the applicability of the approaches discussed herein, in addition to the above frame, here onwards referred to as the healthy system (U1), an additional healthy condition U2 is considered, by adding two masses at the third floor: one on the south and the other on the north floor edge. The training data set is constituted by 89 input-output sets of acceleration histories. Four different "damaged" frames (D1 to D4) are also tested using the same set of 6 inputs. In these damaged frames, structural damage is simulated as stiffness reduction, by replacing one or more columns of the "healthy" frame with columns of reduced cross-sectional area (50.8 $\times$ 7 mm). The testing set consists of 144 data sets: 10 from state U1, 14 from state U2 and 30 from each of the four damaged states.

The results of the stiffness change detection and location are presented in Table 5.2. In Table 5.2, for each state, the ratio n/N indicates the number of tests, n, over the overall tests performed under a certain state, N, for which a change in the given diagonal term of the stiffness matrix is identified; the letter in parenthesis indicates whether that change is identified as due to damage (D)

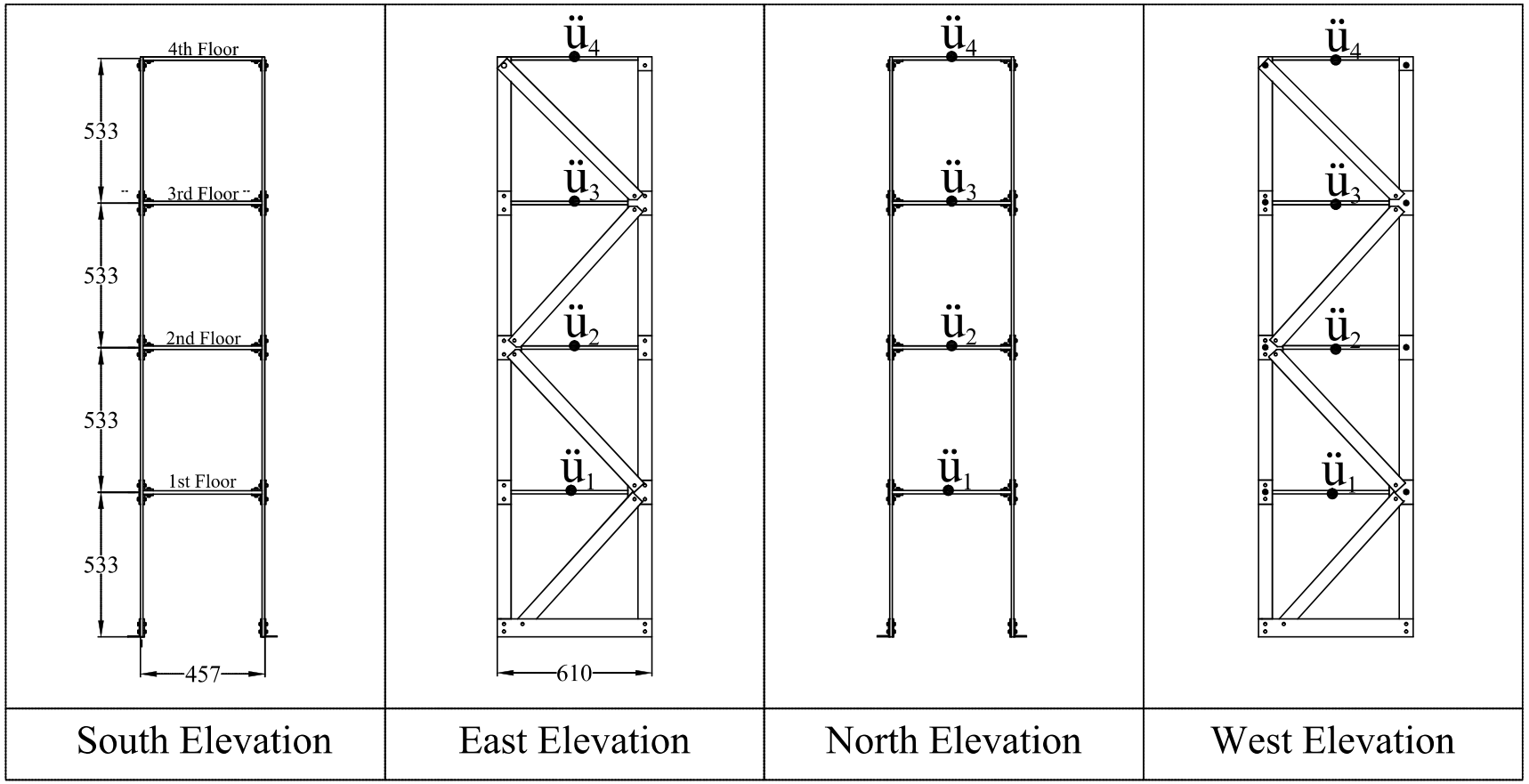

Figure 5.2: Elevation views of the steel frame employed in the experimental application. Dimensions are in mm.

Table 5.2: Results for stiffness change identification and location.

State	$\mathbf{K_{1,1}}$	$\mathbf{K_{2,2}}$	$\mathbf{K_{3,3}}$	$\mathbf{K_{4,4}}$
U1	**2/10 (D)**	0/10	**2/10 (R)**	**1/10 (D)** **2/10 (R)**
U2	0/14	0/14	0/14	0/14
D1	0/30	0/30	**30/30 (D)**	**2/30 (D)**
D2	0/30	**30/30 (D)**	**30/30 (D)**	0/30
D3	**17/30 (R)**	**30/30 (D)**	**30/30 (D)**	0/30
D4	0/30	**21/30 (D)**	**30/30 (D)**	0/30

or retrofitting (R). Type I error, i.e. the error made by declaring damaged the system, when it is instead undamaged, is low and equal to 1.6% (5 out of 306 cases). Adversely, Type II error, i.e. the error made by declaring healthy the structure, when it is instead damaged, is equal to 25.6% (69 out of 270 cases). While damage scenarios D2 and D3 are correctly identified and located with 100% accuracy, the method identifies the stiffness change at DOF 3, but fails at identifying such change at DOF 2 for the damage scenario D1; similarly, for state D4, stiffness change at the third inter-story is identified both at DOF 2 and 3, but the stiffness reduction at the second inter-story cannot be identified from these results. One possible reason behind this misidentification is that both damage scenarios D1 and D3 cause torsion in the system, which may not be captured well by the 4 DOFs 1-D model used. Nonetheless, even in these scenarios the overall system is identified as damaged, and the region containing the damaged elements is identified accurately as well.

Figure 5.3 shows the results of the stiffness change extent quantification. For any DOF, the plot in Figure 5.3 is obtained as follows. Let $d_U^{95\%}$ correspond to the 95th percentile from the upper bound training ECCDF. Such $d_U^{95\%}$ is subtracted from the d's associated with the 144 testing ECCDFs. From the resulting new shifted 144 ECCDFs, the median d values, here onwards referred to as $d_{UT}^{50\%}$, are obtained. Finally, for any given state, the average of such $d_{UT}^{50\%}$ values are computed over all the tests performed on that state, e.g. over the 10 tests on State U1. Comparing the average estimated damage extent displayed in Figure 5.3 with the theoretical values presented in the last column of Table 5.1, it is evident that the proposed approach is able to quantify the extent of stiffness change with reasonable accuracy.

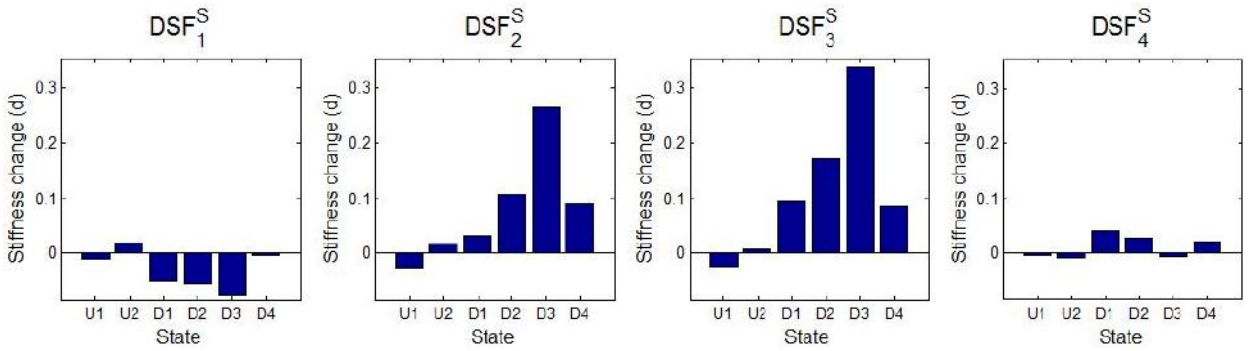

Figure 5.3: Average damage extent for the six states of the experimental application.

An interesting observation from this experiment is the apparent increase in first-story stiffness with damage. The phenomenon may be appreciated in Table 5.2: at DOF 1, for State D3, 17 out of the 30 tests identify an unexpected, systematic increase in stiffness at the first inter-story. Such phenomenon is clearly observable when analyzing the change in stiffness in the tested states shown in Figure 5.3. Such increase in stiffness is less marked for state D4, since the DOF 1 in this state also includes the effect of a damage in the second story; in fact, the average value of the estimated damage extent should be approximately equal to 0.075 in state D4 (Table 5.1). One possible explanation of the first story stiffness increase may be the activation of some strengthening mechanism (e.g. increased participation of the braces in load resistance, particularly strong torsional component, etc.) in the first story when there is damage at some other stories. Such trend is more marked as the damage severity increases: while for damage scenarios D1 and D2 the average stiffness increase at the first inter-story is between 5-6% (Figure 5.3), for damage scenario D3 the increase in stiffness is nearly 8%, causing more than half of the tests performed from this state to be declared retrofitted at the first inter-story (Table 5.2). A similar unexpected increase in stiffness has been observed for the same structure also in [4, 29], where the stiffness properties of the frame structure have been identified using different approaches than the one presented in this report.

6. Summary and Conclusions

In this project, a "mixed" approach for structural health monitoring using ambient/operational vibration response measurements is proposed. This approach is general and can be applied to both bridges and building structures. The DSFs, defined in a model based setting in terms of experimental modal parameters (natural frequencies and mode shapes), attempt to measure relative localized stiffness reductions. The assessment of the structural health is performed in a statistical pattern recognition (solely data based) framework using the DSFs extracted from response measurements. The features in the training stage, extracted from response measurements on the baseline (healthy) structure, in a wide variety of environmental/operational conditions (e.g. in different diurnal/seasonal temperatures, traffic, wind, etc.,), are used to compute a range of ECCDFs, from which lower and upper bound training ECCDFs are estimated. Such a training procedure intends to decouple the normal (non-damage induced) structural variations from damage induced changes, by defining a zone of normal variability of the baseline structural state through the estimated lower and upper bound training ECCDFs. The ECCDFs of DSFs extracted from the data collected in the testing stage are then compared against the lower and upper bound training ECCDFs to assess the presence, location and severity of any change in the structural stiffness parameters. To detect the existence of damage induced changes two methods of analysis are discussed: one based on a measure ($\mathcal{P}$ value) of mismatch between the testing ECCDF and the zone defined by the lower and upper bound training EECDFs, and the other based on three different ratios of the Łukaszyk–Karmowski metric computed using epdfs derived from the testing and upper and lower bound training ECCDFs. The $\mathcal{P}$ value based method performs a two-class classification, i.e. no change vs. change in stiffness at the location under consideration. The method using Łukaszyk–

Karmowski metric ratios instead allows us to perform a three-class classification, i.e. no change vs. reduction (i.e. damage) vs. increase (i.e. retrofitting) in stiffness at the location under consideration, and hence may also be used for verification of retrofitting operations. The results of a numerical example simulating ambient vibration testing of a bridge deck system illustrates that, with the localized definition of the DSF, using either/both the above two methods one may detect and locate the existence of any stiffness change with reasonable accuracy. After the existence and location of change detection, the severity of change is also estimated using the testing and lower and upper bound training ECCDFs. For this purpose the testing ECCDF is adjusted using different percentiles of the two training ECCDF bounds, resulting in a probability box model to represent the exceedance probability for different change severity levels. Such a model consists of a lower and an upper bound curves, representing the probability of change vs. severity of change, using which, for any given change severity a lower and upper bound of the probability of exceedance can be estimated, and vice versa. The numerical example of the bridge deck shows that the severity of stiffness reduction/increase induced by damage/retrofitting may be estimated with reasonable accuracy using such curves. The two level uncertainty in the damage severity attempts to segregate: (a) the uncertainty from measurement noise, input variability, and environmental/opetational variability in the training (healthy) state, expressed through a single exceedance probability of severity of change, and (b) the uncertainty from unknown environmental/opetational conditions in the testing state, expressed through a range of possible values the exceedance probability may take. If the monitored system is fully instrumented, then the proposed DSF and health assessment method allow also an accurate element level change localization and severity estimation, while for partially instrumented systems it successfully identifies a region within which damage is confined.

Acknowledgements

- Dyab Khazem of the Parsons Transportation Group for his valuable contributions, comments and suggestions during the entire project.

- Financial support from the US Dept of Transportation - Research and Innovative Technology Administration (RITA) under award number DTRT12-G-UTC16, through the Center for Advanced Infrastructure and Transportation (CAIT), Rutgers, The State University of New Jersey, award number S1760914.

- PhD students, Luciana Balsamo and Suparno Mukhopadhyay, for their help with the research discussed herein.

- Adrian Brugger, Dr. Manolis Chatzis and Prof. Andrew Smyth for their collaboration during the experimental phase of the work.

Bibliography

[1] F.E. Udwadia, D.K. Sharma. Some uniqueness results related to building structural identification, *SIAM Journal of Applied Mathematics*, 34, 104-118, 1978.

[2] L.S. Katafygiotis, J.L. Beck. Updating models and their uncertainties. II: Model identifiability, *ASCE Journal of Engineering Mechanics*, 124, 463-467, 1998.

[3] S. Mukhopadhyay, H. Luş, R. Betti. Modal parameter based structural identification using input-output data: Minimal instrumentation and global identifiability issues, *Mechanical Systems and Signal Processing*, 45, 283–301, 2014.

[4] S. Mukhopadhyay, H. Luş, R. Betti. Structural identification with incomplete instrumentation and global identifiability requirements under base excitation, (under review).

[5] S.W. Doebling, C.R. Farrar, M.B. Prime, D.W. Shevitz. Damage identification and health monitoring of structural and mechanical systems from changes in their vibration characteristics: A literature review, *Los Alamos National Loaboratory Report* LA-13070-MS, 1996.

[6] C.R. Farrar, K. Worden. Structural health monitoring: A machine learning perspective, *John Wiley & Sons, Ltd*, Chichester, UK, 2013.

[7] K. Worden, G. Manson, N.R.J. Fieller. Damage detection using outlier analysis, *Journal of Sound and Vibration*, 229, 647-667, 2000.

[8] L. Balsamo, R. Betti, H. Beigi. A structural health monitoring strategy using cepstral features, *Journal of Sound and Vibration*, 333, 4526–4542, 2014.

[9] L. Balsamo, R. Betti, H. Beigi. Damage detection using large scale covariance matrix, in *Proceedings of the 32nd International Modal Analysis Conference* (IMAC), Orlando, February 2014.

[10] A.K. Pandey, M. Biswas, M.M. Samman. Damage detection from changes in curvature mode shapes, *Journal of Sound and Vibration*, 154, 321–332, 1994.

[11] O.S. Salawu, C. Williams. Bridge assessment using forced-vibration testing, *ASCE Journal of Structural Engineering*, 121, 161–173, 1995.

[12] P. Cornwell, S.W. Doebling, C.R. Farrar. Application of the strain energy damage detection method to plate-like structures, *Journal of Sound and Vibratio*n, 224, 359–374, 1999.

[13] W.-X. Ren, G. De Roeck. Structural damage identification using modal data. I: Simulation verification, *ASCE Journal of Structural Engineering*, 128, 87-95, 2002.

[14] K.-V. Yuen, J.L. Beck, L.S. Katafygiotis. Efficient model updating and health monitoring methodology using incomplete modal data without mode matching, *Structural Control and Health Monitoring*, 13, 91-107, 2006.

[15] S. Mukhopadhyay, H. Luş, A.L. Hong, R. Betti. Propagation of mode shape errors in structural identification, *Journal of Sound and Vibration*, 331, 3961–3975, 2012.

[16] L. Balsamo, S. Mukhopadhyay, R. Betti. Structural damage detection using statistical pattern recognition with Stiffness Proportional Damage Sensitive Features, in *Proceedings of the 6th World Conference on Structural Control and Monitoring* (6WCSCM), Barcelona, July 2014.

[17] R.D. Nayeri, S.F. Masri, A.G. Chassiakos, Application of structural health monitoring techniques to track structural changes in a retrofitted building based on ambient vibration, *ASCE Journal of Engineering Mechanics*, 133, 1311–1325, 2007.

[18] J. Brownjohn, K.-Y. Koo. Structural health monitoring of Sheffield University Arts Tower during retrofit, in *Earthquakes and Health Monitoring of Civil Structures*, Ed. M. Garevski, Springer, 149–166, 2013.

[19] S. Łukaszyk. A new concept of probability metric and its applications in approximation of scattered data sets, *Computational Mechanics*, 33, 299–304, 2004.

[20] M.W. Vanik, J.L. Beck, S.K. Au. Bayesian probabilistic approach to structural health monitoring, *ASCE Journal of Engineering Mechanics*, 126, 738–745, 2000.

[21] H. Sohn, M. Dzwonczyk, E.G. Straser, A.S. Kiremidjian, K.H. Law, T. Meng. An experimental study of temperature effect on modal parameters of the Alamosa Canyon bridge, *Earthquake Engineering and Structural Dynamics*, 28, 879–897, 1999.

[22] B. Peeters, G. De Roeck. One-year monitoring of the Z24-Bridge: Environmental effects versus damage events, *Earthquake Engineering and Structural Dynamics*, 30, 149–171, 2001.

[23] S. Soyoz, M.Q. Feng. Long-term monitoring and identification of bridge structural parameters, *Computer-Aided Civil and Infrastructure Engineering*, 24, 82–92, 2009.

[24] E. Figueiredo, G. Park, C.R. Farrar, K. Worden, J. Figueiras. Machine learning algorithms for damage detection under operational and environmental variability, *Structural Health Monitoring*, 10, 559–572, 2011.

[25] E. Parloo, P. Verboven, P. Guillaume, M. Van Overmeire. Sensitivity-based operational mode shape normalisation, *Mechanical Systems and Signal Processing*, 16, 757-767, 2002.

[26] A. Hanselmann, O.C. Schrempf, U.D. Hanebeck. Optimal parametric density estimation by minimizing an analytic distance measure, in *Proceedings of the 10th International Conference on Information Fusion*, 2007.

[27] A.L. Hong, F. Ubertini, R. Betti. New stochastic subspace approach for system identification and its application to long-span bridges, *ASCE Journal of Engineering Mechanics*, 139, 724–736, 2013.

[28] H. Luş, R. Betti, R.W. Longman. Identification of linear structural systems usign earthquake induced vibration data, *Earthquake Engineering and Structural Dynamics*, 28, 1449-1467, 1999.

[29] G. Fraraccio, A. Brugger, R. Betti. Identification and damage detection in structures subjected to base excitation, *Experimental Mechanics*, 48, 521-528, 2008.